UNIVERSIDADE FEDERAL DO PAMPA

DALMO PAIM DE OLIVEIRA

FLUID FLOW THROUGH POROUS MEDIA WITH THE ONE DOMAIN APPROACH: A SIMPLE MODEL FOR GRAINS DRYING

Alegrete

2021

DALMO PAIM DE OLIVEIRA

FLUID FLOW THROUGH POROUS MEDIA WITH THE ONE DOMAIN APPROACH: A SIMPLE MODEL FOR GRAINS DRYING

Dissertação de Mestrado apresentada ao Programa de Pós Graduação Stricto sensu em Engenharia da Universidade Federal do Pampa (UNIPAMPA, RS), como requisito parcial para obtenção do grau de Mestre em Engenharia .

Orientador: Prof. Cesar Flaubiano Cristaldo

Alegrete

2021

DALMO PAIM DE OLIVEIRA

FLUID FLOW THROUGH POROUS MEDIA WITH THE ONE DOMAIN APPROACH: A SIMPLE MODEL FOR GRAINS DRYING

Dissertação apresentada ao Programa de Mestrado em Egenharia da Universidade Federal do Pampa, como requisito parcial para obtenção do Título de Mestre em Engenharia.

Dissertação defendida e aprovada em: 19 de novembro e 2021.

Banca examinadora:

_____

Prof. Dr. Cesar Flaubiano da Cruz Cristaldo

Orientador

UNIPAMPA

_____

Prof. Dr. Paulo Carteri Coradi

UFSM

_____

Prof. Dr. Rafael Maroneze

Assinado eletronicamente por **CESAR FLAUBIANO DA CRUZ CRISTALDO**, **PROFESSOR DO MAGISTERIO SUPERIOR**, em 13/12/2021, às 20:01, conforme horário oficial de Brasília, de acordo com as normativas legais aplicáveis.

Assinado eletronicamente por **RAFAEL MARONEZE**, **PROFESSOR DO MAGISTERIO SUPERIOR**, em 13/12/2021, às 20:06, conforme horário oficial de Brasília, de acordo com as normativas legais aplicáveis.

A autenticidade deste documento pode ser conferida no site https://sei.unipampa.edu.br/sei/controlador_externo.php?acao=documento_conferir&id_orgao_acesso_externo=0, informando o código verificador **0693396** e o código CRC **E98DF512**.

Dedico aos meus familiares, amigos, ao meu orientador, colegas de mestrado e de trabalho.

AGRADECIMENTOS

Gostaria de agradecer e dedicar essa dissertação as seguintes pessoas:
Minha Família, minha mãe Paula, meu pai Dalmo, minha avó Shirley que estiveram sempre presente na minha caminhada.
Meus avós Jarlei, Dalmo e Vicente, que neste e mesmo no outro plano sempre me deram suporte.
Meus irmãos Victhor e Juliana a quem dedicaram sua atenção nas minhas mazelas.
Meus tios Ana Glaucia, Elton, Leila, Marcus, Jussara pelo empenho em me proporcionar sempre o melhor.
Meu orientador Cesar a quem me incentivou a continuar mesmo quando o caminho parecia difícil. Ao Mariovani pela disponibilização do codigo inicial.
Aos meus colegas e professores do PPENG pelo apoio, ensinamento e pelos momentos de alegria e descontração.
Aos amigos e pessoas que passaram na minha vida e que deixaram um pouco de si na minha trajetória.
Agradeço, pois diante dos momentos bons e ruins com estas pessoas, me construí e reconstruí, para que hoje, dedicando esse mérito a mim mesmo, eu digo ser capaz de qualquer coisa.

” Respire! Respire e concentre-se no conhecimento que está dentro de você. Os desafios surgem para extrair o que há de melhor em nós.”

Luane Barth Wanderlind

LIST OF FIGURES

LIST OF TABLES

LISTA DE SIGLAS

CFD	*Computational Fluid Dynamics*
$UNIPAMPA$	Universidade Federal do Pampa

LISTA DE SÍMBOLOS

C	Concentration
c_p	Specific Heat, [kJ kg^{-1} °C^{-1}]
c_F	Forchheimer Coefficient
Da	Darcy Number = K/d²
Fr	Froude Number
$\overrightarrow{g}$	Gravity, [m s^{-2}]
k	Thermal Conductivity, [W m^{-1} °C^{-1}]
K	Permeability, [m^2]
α	Thermal Diffusivity (m^2/s)
P	Pressure, [Pa]
Pe	Péclet Number ($Pe = \frac{Lu}{\alpha}$)
L	Characteristic Length
q	Heat Flow by conduction
Q_W	Net work transfer, [W]
Q_{fg}	Latent Heat of Vaporization, [J/kg]
Re	Reynolds number ($Re = \frac{\rho u L}{\mu}$)
Sc	Schimdt Number
t	Time, [s]
T	Temperature
u	Velocity in the direction x, [m s^{-1}]
v	Velocity in the direction y , [m s^{-1}]
U	Velocity vector
x	Direction x from the cartesian coordinates
y	Direction y from the cartesian coordinates
L	Length [m]

μ	Dynamic Viscosity, [kg m^{-1} s^{-1}]
ρ	Density, [kg m^{-3}]
ε	Porosity

CONTENTS

Abstract

Considering that the grain mass is an amount of solid and empty spaces (holes) which a fluid may pass through, one can assume the grain drying as a coupled open-porous medium problem. Mathematical modeling and computer simulation are widely used to describe convection in a free flow with a porous obstacle.This work aimed to model a convection problem through a cylindrical porous media, adopting a single-domain approach. A model of a cylinder containing grains is performed. Inside the grains, there is a certain amount of water, and diffusion of water from inside to the outer of the porous cylinder is also analyzed. A two-dimensional finite volume grid in the cartesian coordinates is used to simulate the sorrounding and inside of the porous cylinder section. The grid consists of 102 nodes in the r direction and 296 nodes in θ. We discovered that the flow field remains steady for the range of Reynolds number considered (1$\leq$Re$\leq$ 40), presenting symmetric and non-symmetric behavior as Re rise. At last, with high Re (Re> 90), destruction of the symmetric pattern (von Kármán vortex street) could be reproduced by our study. The analysis of the concentration plume was done for a better understanding of the wet path in grain drying. Also an important information to help determine the drying rate in future studies.

Keywords: Drying, open-porous medium, single-domain approach, von Kármán vortex street.

Resumo

Considerando que a massa de grãos é uma quantidade de espaços sólidos e vazios (orifícios) pelos quais um fluido pode passar, pode-se assumir a secagem do grão como um problema de um escoamento em meio poroso. Neste sentido, a modelagem matemática e a simulação computacional são utilizadas para descrever a convecção em um fluxo livre adicionando um obstáculo poroso. Este trabalho tem como objetivo modelar um problema de convecção através de um meio poroso cilíndrico, adotando uma abordagem de Single-Domain. Um modelo de secagem de um cilindro contendo grãos é executado. Entre os grãos, existe uma certa quantidade de água, e também é analisada a difusão da água de dentro para fora do cilindro poroso. Uma malha numérica de volumes finitos bidimensionais em coordenadas cartesianas é usada para simular o entorno e dentro da seção do cilindro poroso. A malha numérica consiste em 102 nós na direção r e 296 nós em θ. Descobrimos que o campo de fluxo permanece estável para a faixa do número de Reynolds considerado ($1 \leq$ Re ≤ 40), apresentando comportamento simétrico e não simétrico conforme o aumento de Re. Por fim, com alto Re (Re > 90), a destruição do padrão simétrico (esteiras de von Kármán) pôde ser reproduzida por nosso estudo. A análise da pluma de concentração foi feita para um melhor entendimento do caminho da umidade na secagem dos grãos. Também é uma informação importante para ajudar a determinar a taxa de secagem em estudos futuros.

Palavras-chave: Secagem, meio aberto-poroso acoplado, abordagem de Single Domain, esteiras de von Kármán.

1 INTRODUCTION

The drying is one of the most critical steps in the sequence of the grain process. All of this care is due to the fact that improper drying is the major cause of grain deterioration, although when it happens properly, it ensures grain preservation (BROOKER D.B.; BAKKER-ARKEMA; HALL, 1992). Significant loss of crop in the post-harvest, estimated at 10-25% (FAO, 2010). The drying loss increases proportionally to grain production. In developing countries, projects used to reduce grain losses can achieve a higher grain production, increasing by 10 and 20% of the food available (BALA, 2017).

The total losses are the sum of each one through the step of the post-harvest process. Thus the reduction of losses in one stage may allow a far-reaching effect on the entire reduction of losses (MUJUMDAR, 2014). As the minimum grain losses are reached, at the harvesting or post-harvesting process, the production becomes more potent, and the farmers' economy rises (GOLDSMITH; MARTINS; MOURA, 2015). Programs of shrinking the grain losses may guarantee more food security.

Post-harvest loss affects the quantity and quality of the consumptions and consumables investments. The main factors that favor post-harvesting grain loss are spillage (transport and in the storage), grain breakage (i. e. caused by an overdrying), inefficient recovery, processing factors, machine inefficiency, operator inability, grain deterioration, and pest infestation during the storage (MUJUMDAR, 2006).

The high efficiency of drying control can overcome grain losses. Avoiding overdrying or under-drying is the beginning to avoid drying losses. Spending many resources to predict the ideal grain temperature, air-drying rate, grain humidity, and the time of drying are necessary due to getting better efficiency of the process. These resources, such as experiments, equipment, and labor, make the experimental study more costly. One way to reduce such investments is to use numerical simulations. Numerical solution of equations from fluid mechanics are used to represent, with some assumptions according to initial and boundary conditions, natural and artificial phenomenons (CHAPRA S.; CANALE, 2006). Numerical studies are an important tool to overcome demands of experimentals ones. More evident in grain drying process.

The grain drying is a simultaneous process of heat and mass transfer between grain and air. There is a movement of energy from the hot air-flow through the bulks, by the convection process, which is quickly distributed in the grain mass, vaporizing part of the kernels water. Meanwhile, water within the grain is transferred by the diffusion process as a fluid movement and as a convection process on the wet surface (AMPRATWUM, 1976, PANIGRAHI et al., 2020).

Considering that the grain mass is an amount of solid and empty spaces (holes) which a fluid may pass through, one can assume the grain drying as a coupled open-porous medium problem. Mathematical modeling and computer simulation are widely used

to describe convection in a free flow with a porous obstacle. The prediction of the flow rate passing through and around a porous media may be encountered in many studies in the literature. It uses Darcy's law formulation and its current modifications in the porous part and Navier-Stokes formulation in the open part. However, one has to take into account the abrupt change from the free flow and porous media, creating a transition zone.

There are two main methods of solving the fluid flow in coupled free-porous media.The two-domain method creates two separate regions: one region for the free flow and one for the porous medium and an interface layer is presented. It considers a transition zone where the two domains meet, and since the two domains are coupled, appropriate boundary conditions must be chosen. Another method is the Single-domain approach, and it solves the entire domain only differing spatial parameters, like porosity and permeability to each region (CORNELISSEN, 2016BHATTACHARYYA; SINGH, 2011. The present study assumes no transition zone between the coupled open-porous convection problem. RASHIDI et al. (2013), RASHIDI et al. (2014) investigated the fluid flow around and through a porous cylinder,comparing with the solid one. BOVAND et al. (2015) has also added a porous layer to a solid circular cylinder carried out for minimize vortex sheddings behind. Their results indicated that the drag coefficient decreases with the increasing value of Darcy and Reynolds numbers. It is worth mentioning that, the present models is an initial step towards a future complex modeling of grain drying. Darcy and Reynolds numbers and porosity are compared between solid and porous cylinders. In this sense, a model of a cylinder containing grains is performed. Inside the grains, there is a certain amount of water, and diffusion of water from inside to the outer of the porous cylinder is also analyzed. Thus, CFD scheme implemented in FORTRAN using Finite-Volume in order to simulate and computing the numerical solutions. This work aimed to model a convection problem through a cylindrical porous media, adopting a single-domain approach. Using classical problem of a flow around a circular cylinder obstacle to validate our present numerical code. The increase of the vortex pair with Re is expected, as well as the decrease with porosity. To produce the concentration plume and be able to analyze it with previous studies is presumed.

2 LITERATURE REVIEW

2.1 Grain Drying

The drying is a process made to remove the moisture inside a material, commonly used in food production. The grain drying is a removal of the kernel humidity until the safe moisture content, usually 12-14 % on a wet basis (BALA, 2017). They fall into two types of artificial dryers used in grain production Bin and Portable Dryers. Bin Dryers, as batch dryer, recirculating batch dryer bin, and continuous flow dryer usually work with lower airflow velocities than other kinds, consequently, they are generally more energy-efficient. However, it is slower than most other types of dryers. Batch Dryer Bin is a cylindrical structure with a perforated floor, fulled by a grain spreader, a fan heater unit and, a sweep and an underfloor unloading auger, as shown in the Figure 1. The heater fan starts when grains are placed inside the bin and, as long as it does not achieve the lower average grain moisture content the process does not finish (KROKIDA; MARINOS-KOURIS; MUJUMDAR, 2006). All this process in fixed bed drying presents differents zones of drying: dry layer, drying layer and wet layer. All this process in fixed bed drying presents differents zones of drying: dry layer, drying layer, and wet layer. Which has to be taken into account to determine the drying period. The Dry zone is located on the bottom of the bin and it is the first layer to be dried. The process is finished when the wet zone becomes dried.

There are two ways to dry, first investigates using a high-temperature air through a thin layer less than 1 meter and low-temperature air to deep beds. The second takes many hours or days to finish the process, while thin bed drying takes shorter time (PARRY, 1985).

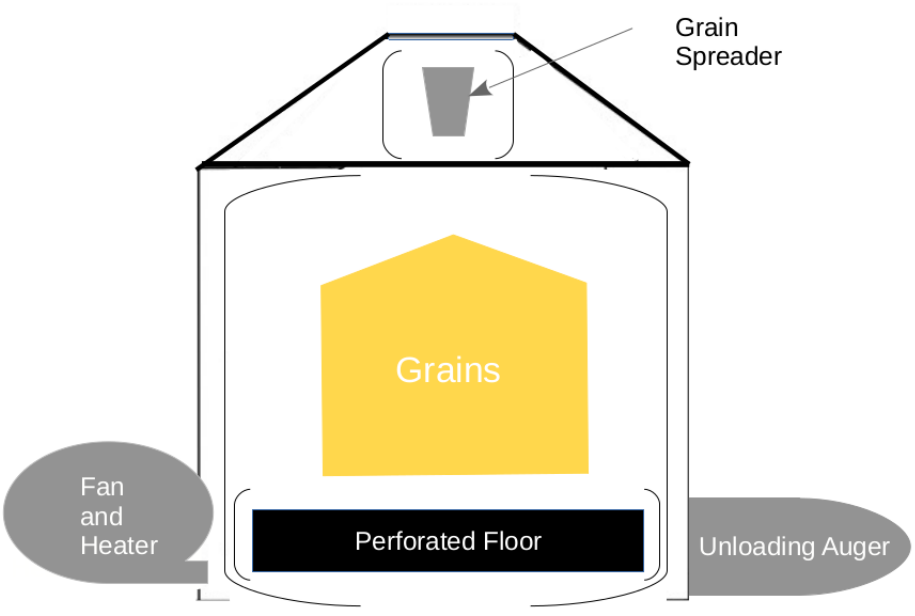

Figure 1 – Batch Dryer Bin.

Drying happens by the application of heat, aimed to maintain the quality of grains during storage, against the growth of bacteria, fungi, virus, and also the development of mites and insects. Besides, the high moisture content leads to grain respiration and germination (BALA, 2017). It can be seen in Figure 2 (FAO, 2010), the relation between moisture content and grain temperature, and how they affect the storability of crops, e. g. to keep the grain in safe storage, when the temperatures are higher, the moisture content has to be smaller.

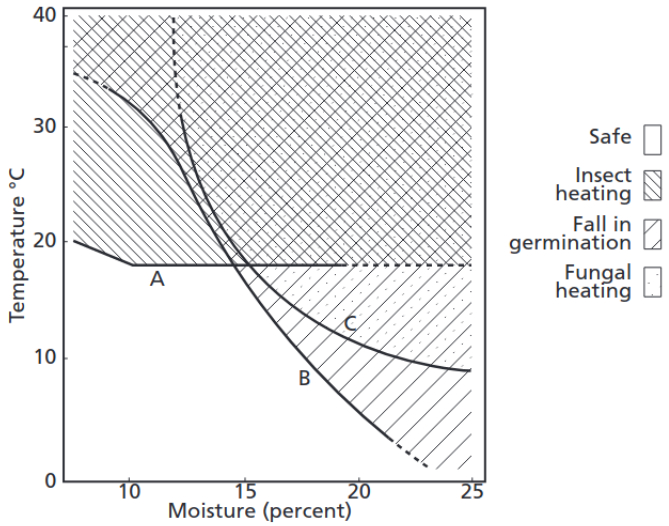

Figure 2 – Effects in the grain deterioration in storage at different temperatures and water content (FAO, 2010).

The dry air is heated naturally or artificially, so it causes a concentration gradient, where the difference in concentration allows the movement of wet from deep inside of the kernel out to the surface. Finally, the airflow carries away the surface moisture and it is evaporated.

The air efficiency of drying, which is the capacity of the airflow catching moisture from a material, depends on the material and air temperature, the relative humidity of the air of drying, and its structure. Just as the supply to drying is grain, the kind of grain species and maturity are an essential influence on the air capacity. The latter serves as an indicator of humidity inside the kernel.

2.1.1 Grain Structure, Composition and Properties

BROOKER D.B.; BAKKER-ARKEMA; HALL (1992) divided the grain drying into two stages, named: constant and falling drying rate periods. At the beginning (constant rate), grain is involved by a film of water, so the moisture evaporates as a free water surface. Then while the surface moisture is evaporating, the surface of the grain will be exposed, and the falling rate period begins. When the surface is no longer wet, some mechanisms of the grain resistance will retard the moisture loss. To better understand the grain drying,

it is necessary take to account all the microscopy structure, composition and properties of the grain, considerable more complex than those for large-scale. The grain layers chemical composition, structure and properties affect the rate of drying, adsorption characteristics and the air flow resistance (BROOKER D.B.; BAKKER-ARKEMA; HALL, 1992).

There exist significant difference in drying rate among varieties and hybrids. The dimension, weight and structure affect their drying behavior. In order to minimize the kernel damage during harvesting and fuel consumption, crop has to be harvested close to the optimal moisture content. Most of the grains, for instance paddy rice, corn and wheat, are usually harvested at moisture between 18% and 35% (wet bulb). And the proper content for storage grains is around 14%. This moisture content is necessary to prevent mold growth and grain germination (CHAUHAN; CHOUDHURY; GARG, 1996)(BROOKER D.B.; BAKKER-ARKEMA; HALL, 1992).

The grains structure has a significant result on the drying rate. When the grains are seen anatomically, even similar, their structure can differ from one another. Therefore, grains like rye, corn, and wheat are composed of pericarp and seed. In which the latter is composed of testa, embryo, and endosperm. Some kernels like rice, barley, and oats have an additional coat of palea and lemma covering, called husk. Figure 3 presents the structure of rice, corn and wheat anatomically.

During drying, moisture flows from the interior to the surface, leaving the grain kernels mainly through the region around the germ, only a small amount of moisture diffuses through the pericarp. The moisture flow depends on the internal characteristics of the endosperm, the permeability of the aleurone layer, and testa and pericarp. Besides that, the process is influenced by the extent of damage to the grain tissues. Thus, broken and cracked grains dry more quickly than whole grains (BALA; BALA, 1997).

A relevant phenomenon that happens in the drying process of any agricultural product is the shrinkage. The volumetric contraction of the grain is due to the decrease in moisture content. It happens with any crop product, the removal of water leads to a reduction of the tensions inside the cells of the tissues, producing its shrinkage (PRADO; ALONSO; PARK, 2000)(RESENDE et al., 2007)(SADAKA; ATUNGULU; OLATUNDE, 2016). SEIFI; ALIMARDANI (2010) studied about dimension reduction after the dehydration of the corn. They reported that the higher the humidity, the greater the physical properties of the grains become. Average properties such as length, width, thickness, geometric mean diameter, sphericity, thousand grain weight, angle of repose, grain volume, surface area, bulk density, porosity, and aspect ratio increased with the increasing moisture. Some works, as Bala (1983) created a mathematical hypothesis of a grain bed to found the maximum possible shrinkage, also developing an experimental equation to the coefficient of shrinkage. According to BALA; WOODS (1984) and BALA; BALA (1997), the shrinkage rate in the grain bed decreases gradually, achieving almost zero at very low moisture content. This is caused by the influence of the free shrinkage of particles that compose grain bed and the

elastic shrinkage.

Some simulating models, as CHAUHAN; CHOUDHURY; GARG (1996), assume the volume shrinkage is negligible during the drying process, i.e., the density of the grain remains constant and uniform. The present work, about a simulation of a single kernel drying, supposes that the shrinkage effects can be neglected.

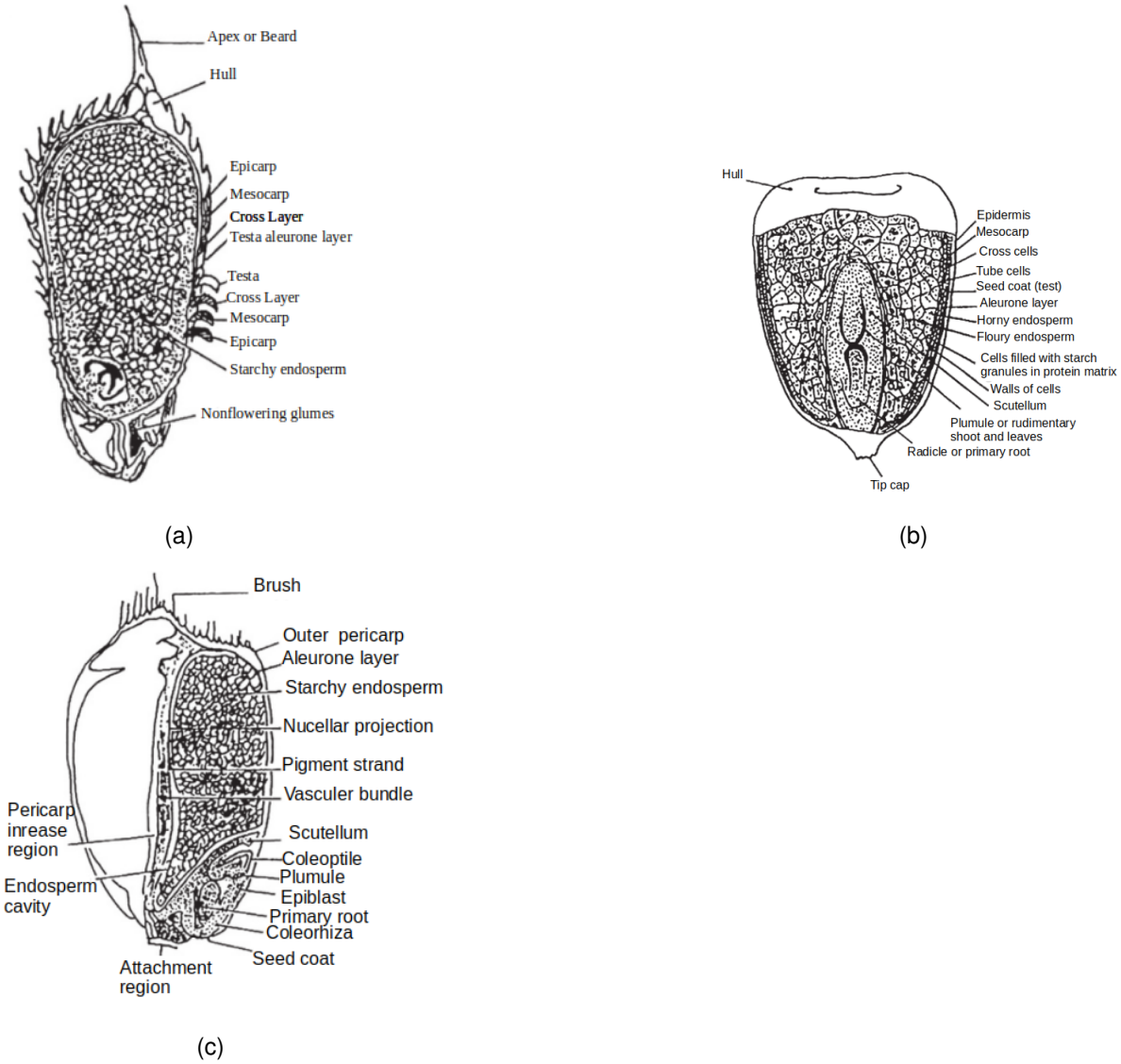

Figure 3 – Structural composition of (a)rice, (b)corn and (c) wheat (Bala et al., 2017)

Therefore, the porosity of the kernel, the void space within the grain tissues (solids) expressed as a percentage of the total volume of the grain, remains constant and uniform as well. Find more information about porosity later,as work goes.

2.1.2 Grain Thermal and Physical Properties

The thermal properties are essential to any mass and heat transfer to simulate the diffusion of water inside a kernel or bulks of kernels. In all the heat transfer during the drying

and storage of grains studies, it is vital the use of the specific heat at constant pressure (C_p), latent heat of vaporization (Q_{fg}) and thermal conductivity (k). Specific heat describes the energy required to increase one degree of temperature. According to Bala et al. (1997) and RAGHAVAN, 2020 when a system (solid or liquid) is in a high pressure, specific heat does not have much influence on pressure. Moreover, in ordinary temperatures and over little temperature intervals conditions, specific heat may be considered as a constant physical property.

General works, as KAWUYO; AVIARA; OKOLO (2019), CAO; NISHIYAMA; KOIDE (2004), SABLANI; RAMASWAMY (2003), CHUMA et al. (1981), aimed to determine a linear regression equation by experimental data with crops thermal properties. It is due to the fact that for wet grains, the behavior of heat capacity is increasing proportionally with the moisture.

The heat flow respects the conservation laws, forming the differential equation that describes the thermal conduction, as shown:

$$\frac{\partial T}{\partial t} = \alpha \left(\frac{\partial^2 T}{\partial r^2} + \frac{1}{r} \frac{\partial T}{\partial r} \right), \tag{1}$$

α been the thermal diffusivity (m^2/s), and it is function of the thermal conductivity K and specific heat capacity (C_p), $\alpha = \frac{K}{\rho C_p}$. Thermal diffusivity means how rapid heat can spread through the material under transient conduction of heat transfer. Fourier Law for heating condition assumes that in any material in which exists temperature difference, the heat flux per unit time per unit area is proportional to the gradient of temperatures in that direction. The Eq. 1 is correct when it is admitted that there is no internal heat been generated, and the thermal conductivity is constant and uniform. As a stady state method of determine the heat flow by conduction, Fourier law becomes:

$$q = -kA\frac{dT}{dn}, \tag{2}$$

n is any direction of the heat flux. The reason for the negative sign in the Fourier equation is due to the direction of the increase in distance n must be the direction of the positive heat flow.

Countless works usually determined the heat conductivity for various species of grains using experimental methods. These authors show a linear increase of the thermal conductivity with moisture content, statistically more significant than temperature, as shown in Table 1 (IGUAZ et al., 2003)(TAVMAN; TAVMAN, 1998) (DESHPANDE; BAL; OJHA, 2007) (ANDRADE et al., 2004). Furthermore, this information is used in several studies, principally for drying and storage modeling of grain beds (MARTINEZ, 2019)(HAMMAMI; MABROUK; MAMI, 2016)(CARRERA-RODRÍGUEZ et al., 2011). Some important physical properties for common grains, based on ASAE (1993), are given on Table 2. Grain porosity

Table 1 – Thermal Conductivity of Grains.

Grains	Moisture (% d.b.)	Thermal Conductivity (W/m K)
Rice (medium-grain)	13	0.0955[1]
Wheat (Eregli)	9.3	0.159[2]
Soybean (whole)	8-25	0.1157-0.1756[3]
Corn	15.8	0.169[4]

[1].aprox. 22ºC (IGUAZ et al.,2003).
[2]. (TAVMAN; TAVMAN, 1998).
[3]. (DESHPANDE; BAL; OJHA, 2007).
[4]. (ANDRADE et al., 2004).

Table 2 – Physical Properties of Grains

Grains	Cultivar	Moisture (% w.b.)	Porosity	Particle Density (Kg/m^3)
Corn	Yellow, dent	25.0	0.44	1270
Soybean	Wilson	7.0	0.338	1130
Rice	Honduras	11.9	0.504	1110
Wheat	Turkey, winter	9.8	0.426	1300

Source: from ASAE, 2003.

was obtained by the relation of bulk density and particle density.

2.1.3 Drying-Air Properties

The most air-flow in the grain drying is composed of a mixture of dry air and water vapor. The dry air contains several gases, mainly oxygen and nitrogen, and avapor. The dry air contains several gases, mainly oxygen and nitrogen, and small amount of argon, carbon dioxide and neon (BROOKER D.B.; BAKKER-ARKEMA; HALL, 1992). The function of the airflow is to provide the required energy to remove the moisture inside to the grain. Moreover, it has to carry the evaporated water out of the kernel mass (HUI, 2008). Some thermodynamics properties of the moist air are analyzed in grain drying, intending to describe the amount of water vapor held in the drying air. It has to represent the air's thermal conditions take into account the Vapor Pressure, Relative Humidity, Humidity Ratio, Dry-bulb Temperature, Dew Point Temperature, Wet-bulb Temperature, Enthalpy, and Specific Volume.

2.1.4 Models of Batch of Grains Drying

Some batch (or fixed beds) drying models are reported since our 50s when a simple method, known as the logarithm equation later, they were used to described moisture movement and temperatures. The rate of moisture and temperature were functions related to depth, which results in low accuracy (SUN; WOODS, 1997). Many studies using one-

dimensional computational fluid dynamics (CFD) have been applied to grain drying, as for example ZARE D; MINAEI; KAOSHTAGHAZA (2006) and EMADI; ZARE (2014), whose works aimed to develop non-equilibrium mathematical and simulation models to rough rice drying in a bed batch dryer, using iterative finite difference method. NAGHAVI; MOHEB; ZIAEI-RAD (2010) presented a numerical simulation of rough rice drying in a deep-bed dryer using non-equilibrium model, mass and energy balance inside a control volume. In this model, it was assumed a set of four non-linear partial differential equations and defined initial and boundary conditions.

SRIVASTAVA; JOHN (2002) develop a model to deep bed grain drying, using semi-empirical equations for predicting air temperature and humidity, air and grain temperature varying through position and time, of a fixed bed of grains. THORPE (2008) demonstrates some modifications to apply CFD to the process of grain stores and the distribution of grain temperature and humidity in an aerated bulk of grain. His study applies some modified CFD codes to account for the grain drying process, to simulate heat and mass transfer through bulks grains. EMADI; ZARE (2014) developed user-defined functions (UDF) to be used in the Fluent software (Fluent Inc., Lebanon, NH), analyzed the performance of energy and exergy to determine the efficiency of the thermal system, and thus it was possible to simulate the deep-bed paddy drying process. Other theories to predict heat and mass transfer through a bulk of grains use diffusion theory and embrace both thin layer drying and deep bed drying. The first one explains a thin wet grain bed media being drying with heated air flow and its behavior. There is no humudity and temperature gradient. The dry of most material is started as a continuous rate, nearly a free water surface, followed by a linear decay of the drying rate. Grains are usually dry during this second decay period. A constant rate period is noted at the beginning of the deep bed drying, and when deep enough the air becomes saturated getting at the wet-bulb temperature of the mass (PARRY, 1985).

The partial differential equation models are often used to afford a more suitable description, despite solving analytically, numerical integration in space and time has to be used. Some authors, as ELGAMAL et al. (2015) and ELGAMAL, KISHK and ELMASRY (2017), use an equilibrium model to represent convective heat and mass transfer in a deep bed of rough rice. Their model applies the conservation of heat and mass to an intra-kernel domain and creates a matrix of various grains being coupling by coefficients of heat and mass of air and grain. Then both energy and mass conservation equations to grain and dryer air were used simultaneously. These coefficients were determined by CFD model are used to porous media, using a representative ellipsoid surrounded by 16 more ellipsoids solids. The distance of the rough rice kernels for each other was chosen to respect the porosity of 50% in the porous media. The momentum conservation equation was not considered, thus no velocity gradient through the porous medium was taken to account.

In addition to the mass and energy conservation equation, SITOMPUL, ISTADI and

SUMARDIONO (2003) worked with momentum conservation to determine the effect of the flow velocity distribution on the drying process. Thus, it was compared with moisture and temperature profile, determined with heat and mass balance in drying gas and grain phase. These governing equations made from Navier Stokes were applied to porous media, which momentum equating employees volume averaging approach described by Liu and Masliyah (1999). The author added a friction factor, which is caused by the slip velocity between the solid and the gas phase. Governing equations for CFD are shown below, and afterward, their applicability to the flow passing through a porous media.

2.2 Porous Media

The study of a flow through a porous media is very important for engineering, for instance to the Reservoir Engineering, where there are many works trying to simulate oil extraction in a reservoir. This oil reservoir simulation, point out to several fields of study aimed at oil production such as: planning, maximizing process efficiency, study of feasibility and advanced fluid recovery study (KAVIANY, 1995).

The uses of porous media analyzes are, as well, to represent natural phenomenons such as water infiltration, percolation, and lixiviation into the soil dealing as a fluid flow through a porous solid. Therefore, as the water into the soil is considered a diffusing substance, we may consider the same for many other examples, for instance, grain drying. The process of grain drying involves continuous heat and mass transfer between solid (grain or grains) and fluid (hot air and vapor). Considering that in the grain drying, the hot air flow takes place through a big batch of solids and holes, we can introduce the idea of a flow of fluid through a porous medium. A porous medium is defined as a space occupied of a matter in a solid and gaseous phase or solid and liquid phase. One of the important characteristics is that the solid matrix's specific surface is relatively high, and the void spaces, called pores which is fulled of fluid, is relatively narrow. Also, the void spaces have to be interconnected, that permits the flux of fluid through them (BEAR, 1968). Thus, one has to take to account not only the porosity but permeability as well.

First of all, one has to define which properties best represent porous medium when a simulate implementation occurs. These properties are: surface area, porosity,pore size distribution, tortuosity and interconnectivity. Pore size distribution and interconnectivity as primary characteristics. These may allow the implementation in a simulate tool as the virtual porous medium to present the characteristics needed to have representativeness of the real environment. Pores are elements that represent the connecting elements within the medium. And as the virtual entity that allows two adjacent empty spaces have interrelationship. Porosity is difined as:

$$\varepsilon = \frac{\textit{void space in the porous medium}}{\textit{total volume of porous medium}} \tag{3}$$

The interfacial area between the fluid and solid phases, identified as $A_\beta\sigma$, will serve as the first assumption called no-slip boundary condiction:V_β = 0, on $A_\beta\sigma$. Where V_β is the velocity on the solid surface. Thus, the fluid flows in a nonorderly direction.

We can consider this flow's characteristics as multiphase transport because the domain is composed of a solid phase and fluid phase. Therefore there is an approach called volume averages models used to obtain some solvable governing equations to predict the macroscopic properties of a multiphase system. One of the types of volume averages commonly encountered in the study of multiphase flow, used in the formulations of Darcy's law, is the phase average. Since the volume element includes different phases, information about the spatial variation of ψ for each phase individually is lost, and $\langle\psi_\beta\rangle$ represents the average for all phases (FAGHRI; ZHANG; HOWELL, 2010). It is defined as:

$$\langle\psi_\beta\rangle = \frac{1}{\Delta V}\int_{\Delta V_B} \psi_\beta \, dV, \tag{4}$$

ΔV_β is representing the volume of the β phase, contained within the averaging volume ΔV. It may depend on the structure of the porous medium of the domain, besides this is only a function of the spatial coordinates for a rigid porous medium. A special concept to work with porous media is that its representative elementary volume has to be much larger than the pore-scale but considerably smaller than the length of the macroscopic domain (BEJAN A.; KRAUS, 2003). The principles of heat and fluid flow through the porous medium saturated with some liquid or gas have to take into account important properties such as porosity and permeability of the porous medium. The velocity through a porous media, supposing its homogeneity and just in direction x, is based on a simplification of the momentum conservation law for a laminar, incompressible, permanent flow, and low Reynolds number.

2.2.1 Darcy's Law

Darcy's law is a phenomenologically derived constitutive equation that describes a fluid flow through a porous medium. The law was formulated by Henry Darcy based on the results of experiments on the flow of water through beds of sand, ATANGANA, 2018. This law represents a proportional association between the instantaneous discharge rate, the viscosity of the fluid, and the pressure drop over a given distance, as shown below:

$$Q = -\frac{K_p A(p_b - p_a)}{\mu L}, \tag{5}$$

in which Q is the total discharge (unity: volume per time), K_p is the intrinsic permeability, which t depends on the geometry of the medium, A is the sectional area of the flow, $(p_b - p_a)$ is the total pressure drop, μ is the viscosity and L is length over which the pressure drop is taking place. The negative sign is because fluid flows from hight to low pressure. Equation

(5) is an observational relation analogous to Fourier's law in the of heat conduction, Ohm's law of electrical networks, and Fick's law in diffusion theory. But the Darcy equation can be derived from Navier-Stokes equations. Equation (5) can be rewritten as

$$\nabla P = -\frac{\mu}{K_p}\mathbf{U}, \tag{6}$$

in which $\mathbf{U} = Q/A$ is the flux discharge per unit area, with units of length per time, named Darcy flux or Darcy velocity. Note that, K_p can a second-order tensor. Equation (Eq.(6) states a linear relationship that is characteristic of the Stokes flow (viscous force dominates over inertial force). However, when the inertial force dominates over the viscous force, a quadratic term is introduced into Eq.(6), named Darcy-Forchheimer equation (described later). Generally, Forchheimer term is necessary when the porous media is highly permeable. The Reynolds number (Re) based on the average pore velocity u_p and an average characteristic length scale for the pores is way to classify the flow regime. The Darcy's Law is valid for $Re < 1$. When Reynolds increase, $0 < Re < 1$, steady nonlinear laminar flow begins and Forchheimer term is necessary. This, equation, imposes limitations on the range of validity of Darcy's law, which was valid for flows with low Reynolds number. In order to account for the high velocity, the Brinkman model, which is an extension of Darcy's model, has been considered. The Brinkman equations commonly describe transitions between slow flow in porous media that is governed by Darcy's law and fast flow described by the Navier Stokes equations. When a convection problem dealing with flow in porous media is described by an analogy with the Navier–Stokes equation, and Dupuit–Forchheimer relationship is used, the Eq. 6 becomes:

$$\rho\left[\frac{1}{\varepsilon}\frac{\partial \mathbf{U}}{\partial t} + \frac{1}{\varepsilon^2}(\mathbf{U}.\nabla)\mathbf{U}\right] = -\nabla P - \frac{\mu}{K_p}\mathbf{U}. \tag{7}$$

The increasing order of Darcy's law when adding the term $(\mathbf{U}.\nabla)\mathbf{U}$ because the spatial derivates, it is not a satisfactory way to describe the inertial effects drag since the term goes to zero in a steady, incompressible and unidirectional fluid (BECK, 1972). The $(\mathbf{U}.\nabla)\mathbf{U}$ term is generally small in comparison with the quadratic drag term (Forchcheimer effects) and it becomes negligible (NIELD; BEJAN, 2017). Thus Eq. 7 be arranged in the form:

$$\rho\frac{1}{\varepsilon}\frac{\partial \mathbf{U}}{\partial t} = -\nabla P - \frac{\mu}{K_p}\mathbf{U}. \tag{8}$$

2.2.2 Forchheimer-Brinkman Modifications

Darcy's equation Eq. (5) is a linear relationship between velocity and pressure. This relationship holds when the Darcy (or seepage) speed is in order unity (low Reynolds num-

ber). Even though no flow transition from laminar to a turbulent state happens, due to the low Reynolds Number within the porous, the breakdown in linearity is because the drag (due to solid obstacles) becomes comparable with the surface drag (due to friction)(NIELD; BEJAN, 2017). The Darcy's law does not take into account no-slip conditions on the solid phase boundary (velocity components equal to zero at surface). Another problem of this approach is its lower order when contrasted to that of the Navier-Stokes equations in flow through porous and free region problems. Some models created in the past fifty years reach in some solutions to the boundary of the interface between porous and free medium, later approved the Forchheimer approach (COSTA et al., 2004; BECKERMANN; VISKANTA; RAMADHYANI, 1988). Darcy's law neglects the inertial effects due to the pressure drag (region behind the particles in a stream). JOSEPH; NIELD; PAPANICOLAOU (1982) developed a formulation accounting the inertial influences in the flow in the porous media, i. e., the inertial resistance is proportional to the quadratic of the velocity (Dupuit-Forchcheimer suggestion). Thus, Eq. 6 becomes:

$$-\nabla P = \frac{\mu}{K_p}\mathbf{U} + \frac{c_F}{{K_p}^{1/2}}\rho|\mathbf{U}|\mathbf{U}, \tag{9}$$

C_F is known as Forchheimer coefficient,a cylinder full of solid spheres C_F is defined as (BOVAND et al., 2015):

$$C_F = \frac{1.75}{\sqrt{150\varepsilon^3}}. \tag{10}$$

Only the damping force of the porous mass has been retained in Darcy's law, then viscous shearing stresses are neglected. BRINKMAN (1949) also developed an additional viscous term to Darcy's equation derived from the Navier-Stokes equation for viscous flow ($\mu_e\nabla^2 Q$). The addictionals viscous terms are added to Eq. 9, as shown below:

$$-\nabla P = \mu_e\nabla^2\mathbf{U} + \frac{\mu}{K_p}\mathbf{U} + \frac{c_F}{{K_p}^{1/2}}\rho|\mathbf{U}|\mathbf{U}, \tag{11}$$

in which μ_e is the effective viscousity, considered iqual than μ by Brinkman ($\mu_e/\mu = 1$). Eq. (11) is know as Brinkman's modification. For beds of particles, one can introduce an effective average particle diameter D_p. The hydraulic radius theory of Carman-Kozeny leads to the relationship based on experimental results looking a best fit to Permeability (K) (NIELD; BEJAN et al., 2006):

$$K = \frac{D_p^2\varepsilon^3}{180(1-\varepsilon)^2}, \tag{12}$$

where D_p is the characteristic diameter of a particle in the porous cylinder (BHATTACHARYYA; DHINAKARAN; KHALILI, 2006).

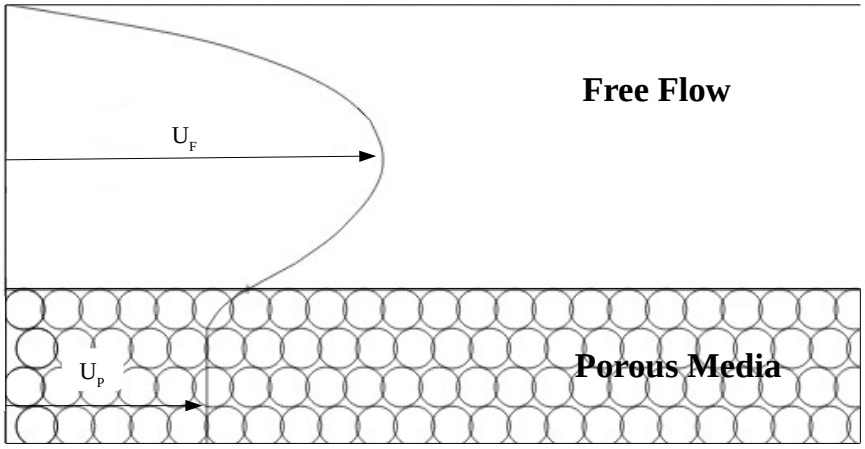

Figure 4 – Coupled Free-Porous Flow with Two-Domain Approach (GOYEAU et al., 2003).

2.3 One-domain approach to Fluid Flow coupled in Free-Porous Medium

There are two methodologies to solve a free fluid flow coupled with the porous region, adopting separating, or not, two homogeneity regions (or subdomains). The first region is a Stokes problem, which solves for the fluid velocity and pressure in the free flow domain. The second is a modified Darcy problem for the Darcy pressure in the porous medium. The first approach, called Two-domain, applies two distinct sets of equations written in each sub-space, models the free fluid flow zone with Navier-Stokes equations and the fluid in a porous zone with Darcy equation (LAYTON; SCHIEWECK; YOTOV, 2002). In this method, a transition interface between free fluid flow and Porous fluid flow has to be taken into account, and also proper explicit boundary conditions at the interface. Slip boundary conditions must be applied at the interface since Navier-Stokes and Darcy's equations are of different orders (BABER, 2014, CHIDYAGWAI; RIVIÈRE, 2011). Figure 4 shows a coupled problem of fluid flow through and over a porous layer solved by the Two-Domain approach, transition interface is not neglected. BEAVERS; JOSEPH (1967) established that a viscous fluid flows passing parallel porous medium surface effects of viscous shear (such as Brinkman's effects) in the fluid will penetrate beneath the permeable surface. This is the reason the porous medium induces a boundary layer region, also called the intermediate interface.

Some methods must be used to get the behavior of the flow in the transition layer.

Pore-network model is one of them, used to solve flows in the transition interface that couples free-flow and porous media flow, as the work of CORNELISSEN (2016). The Single or One-Domain Model runs in the entire domain (Free, Porous and Interface) but alternates different spatial parameters, as permeability and porosity, to each region. Then, a single set of equations is written for whole domain incorporate the free fluid and homogeneous porous regions, and the interface. The sharp transition happens with the modification of these spatial parameters. There is no need to apply coupling conditions since the transition zone is described only with the modifcation of these phisical parameters (CORNELISSEN, 2016). In the open region, the Darcy term disappears since the permeability must be considered infinite, and the porosity becomes high ($\varepsilon = 1$). Thus in the open region, the Navier-Stokes model is predominant. The porous region is considered a pseudo-fluid and the composite region is treated as a continuum when Darcy term is predominant. JUE (2004) studied flow fields over a porous and saturated square cylinder with variation of porosity and Darcy number using single-domain approach. It accounted for viscous and inertial effects in the porous region, which aimed to characterization of vortex shedding ganerated. According to JAMET; CHANDESRIS; GOYEAU (2009), the interface of the Single-Domain can be either a continuous and discontinuous transition zone, in which the physical variables pass across in continuous variations or a discontinuous variation. GOYEAU et al. (2003) compares the Single and Two-domains to a stationary problem, incompressible fluid and neglected inertia effects in both regions. In free fluid flow, Navier-Stokes equation becomes predominant, while in Porous media Brinkman modification equation does. The spatial variation of the properties (porosity, permeability and effective viscosity) was made continuously.

SILVA; LEMOS (2003) has been worked with a laminar fluid passing under a porous media, considering inertial effects (Forchheimer's effects), and implementing a jump condition since there is a discontinuity interface between both regions. When variables are not continuously differentiable in the whole domain, jump conditions are required by governing laws at the transition stress zone (HOLLAR, 2018). OCHOA-TAPIA; WHITAKER (1995 focused only in the determining jump condition of the boundary zone between a clean and porous media flow.

JAMET; CHANDESRIS; GOYEAU (2009) proposed to distinguish the Two-domain and the discontinuous One-domain approaches. For the sake of solving with the One-domain approach, it was adopted Heaviside functions to switch on Darcy's modifications in the porous media region. It developed the Darcy-Brinkman equation in the entire domain, prevailing Darcy terms only when Heaviside function was "on". Jump conditions on the Temperature and Heat flux (Dirac delta functions) at the interface are accounted for discontinuous one-domain approach. However, no inertial effect was accounted for. For a homogeneous porous layer, the latter representation and the formulation of the two-domain models were equivalent.

CHANDESRIS; JAMET (2006) proposed the addition of the Forchheimer Law term

to account for the inertial effects, in a free fluid flow over a porous media problem. In the One-domain approach, the transition zone has been achieved by continuous spatial variations of properties, since the boundary between the porous medium and the free fluid is a sharp interface idealization where the properties of the medium encounter strong but continuous variations. CHEN; WANG (2014) studied the momentum transport described by Darcy's law with Brinkman correction, neglecting inertial effects. The interface was considered as a thin transition layer, which across the porosity and permeability suffer a sharp but continuous change. The method of matched asymptotic expansion (MMAE) was used to solve the transition region. Results showed that the one-domain approach has satisfying accuracy in comparison to the two-domain approach. MAHDHAOUI; CHESNEAU; LAATAR (2017) dealt with a free fluid channel flowing through and around a porous cylinder problem, applying the one-domain method. A forced two-dimentional incompressive and laminar flow described by Navier-Stokes in the open region and the Darcy-Brinkman-Forcheimer model in the porous media.Then inertial and viscous forces are taken into account, but no interface does. A set of equations were used to the entire domain, although the only property applied to delimit the porous media was the porosity. Furthermore, the corrections of Darcy's Law for porous media were applied also in the free medium, along with the assumption that in the free flow Da was supposed to be equal to 1. The present study has also assumed no transition zone between the coupled open-porous convection problem. Proposing to model a convection flow through and around a cylindrical porous media, adopting a single-domain approach.

2.4 Fluid flow across circular cylinders

The flow around circular cylinders includes known phenomena, such as separation, vortex shedding and the transition to turbulence (ZDRAVKOVICH, 1997 ZHANG et al., 2016). The mechanisms of vortex shedding and its suppression have significant effects on the practical engineering projects:offshore/onshore structures, bridge piers, and pipelines. Figure (5-a) shows a flow with small Reynolds number $Re < 5$ (regime of unsepared flow). The shape of every streamline is symmetrical around of the cylinder (KWON; CHOI, 1996). When the reynolds number increases $5 < Re < 40$, a fixed pair of vortices is formed. Under this condition, the fluid in the upper half of this region rotates clockwise, whereas the fluid in the lower half rotates counter clockwise, see Fig. (5-b).

Increasing the Reynolds number, the vortices are streched and elonged until $Re \sim 40$. Afterwards, the vortices became unstable and the first periodic forces begin. Thus, a non-symmetric wake develops spontaneously, followed by shedding of vortices ($90 < Re < 150$), as shown Fig. (5-c). At high Reynolds number ($Re > 150$) the fluid flow is in the transition range of turbulence, called von Kármán vortex street (PARK; LADD; HENDRICKS, 1994). The origin of the destruction of the symmetric pattern can be explained by the presence of multiple perturbation sources in the physical model: non-uniform inlet conditions

; irregularity of the boundary conditions (e.g. the surface roughness); perturbations in the running conditions of the experiment (e.g. vibrations). Few authors have been focused on compare drag and vortex shedding behind solid circular cylinders and porous circular ones, in a flow channel. Even porous layers applied in cylinders surface (pipes) have also been used to reduce heat transfer and vortices behind them (BHATTACHARYYA; SINGH, 2011; BRUNEAU; MORTAZAVI, 2008). It occurs since the porous layer minimizes the pressure drop and skin friction which leads to a reduction in drag shedding when it is compared with a solid cylinder. When the velocity in the boundary layer is reduced by the presence of porous media, it leads to a lower heat transfer rate as well (NAZAR et al., 2003).

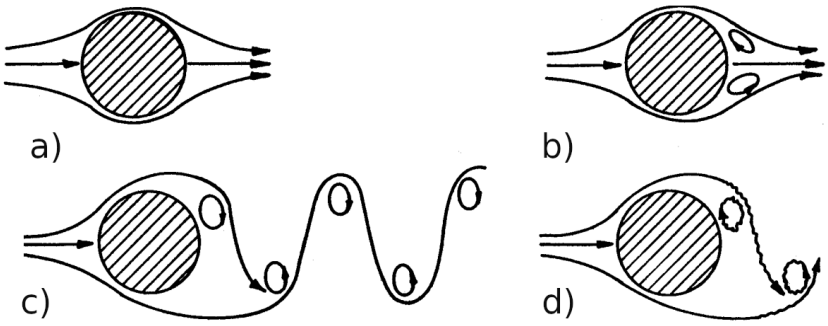

Figure 5 – Regimes of fluid flow across circular cylinder

RASHIDI et al. (2013) worked with flow and heat transfer around a cylinder covered by a superficial homogenous porous layer (porous ring). Two sets of equations were used on the free flow region and the porous region, Navier-Stokes and Darcy's modifications (Brinkman-Forchheimer) respectively. Besides verification of the porous layer as a thermal isolator, the work aimed to analyze the formation of drags shedding and its behavior along the variation of Permeability and Da. No boundary conditions were used for the velocity, temperature, and shear stress at the interface region since the assumption in the interface between the porous and the fluid region was their continuity.

BOVAND et al. (2015) simulated free flow around a porous circular cylinder using Two-domain approach, with Navier-Stokes in the clean domain and Brinkman–Forchheimer formulation was used to model the flow into porous media (adding a magnetic field term). Some interfacial conditions were added to describe the transition between Free flow and through Porous media. Physical parameters, such as the Darcy, Stuart and Reynolds numbers were analyzed in their different values. The results showed up that, for a small Darcy number (Da) (lower than 10^{-6}), the vortex shedding and drag coefficient are similar to that large as of a solid cylinder. Vortex length decreases by the increase of Da because the separation is delayed with the increase in the Darcy number. The increase of permeability causes more suppression of the vortices. This means the increase of resistance to fluid flow in the porous zone with the decrease of the permeability. The present study proposes similar analyses with BOVAND et al.'s work. However, the formulation was based on the

One-Domain Approach to solve the free-porous media problem, and no interface condition was developed. Vortex shedding is analyzed comparing both solid and porous circular cylinder. Heat and Mass transfer, using grain properties, is studied in a way to simulate grain drying.

BHATTACHARYYA; DHINAKARAN; KHALILI (2006) investigated numerically a flow transport through and around a porous cylinder with Re between 1 and 40 with Darcy number (Da) in the range 10^{-6} and 1,5 simulating a marine-related application case, which is a sinking porous aggregates problem (ε from 0,629 to 0,99).

Reattachment length or length of the wake was used to describe the change of vortex dimension when different Re and over time. The reattachment length (or lenght of the wake) L/d (Fig. 6) is defined as the distance from step-down to reattachment point formed behind the cylinder, from the rear of the cylinder to the end of the separated region. DENNIS; CHANG (1970), RASHIDI et al. (2013), BHATTACHARYYA; DHINAKARAN; KHALILI (2006), and BRAZA; CHASSAING; MINH (1986) compared the Reattachment Length obtained in their works with the literature. DENNIS; CHANG (1970) have obtained solutions of the equations of Navier Stokes for steady incompressible flow around a circular cylinder. A range of Reynolds numbers from 5 up to 100 was chosen, thus the length of the wake grew approximately linearly with Re over the whole chosen range. Therefore, their results were in excellent agreement with the literature results. D'ALESSIO; DENNIS (D'ALESSIO; DENNIS) developed a vorticity model to a steady two-dimensional flow of a viscous incompressible fluid past a solid cylinder. The governing Navier-Stokes equations are then solved numerically and good agreement is found with existing results on the literature, particularly in the case of flow past the elliptic cylinder.

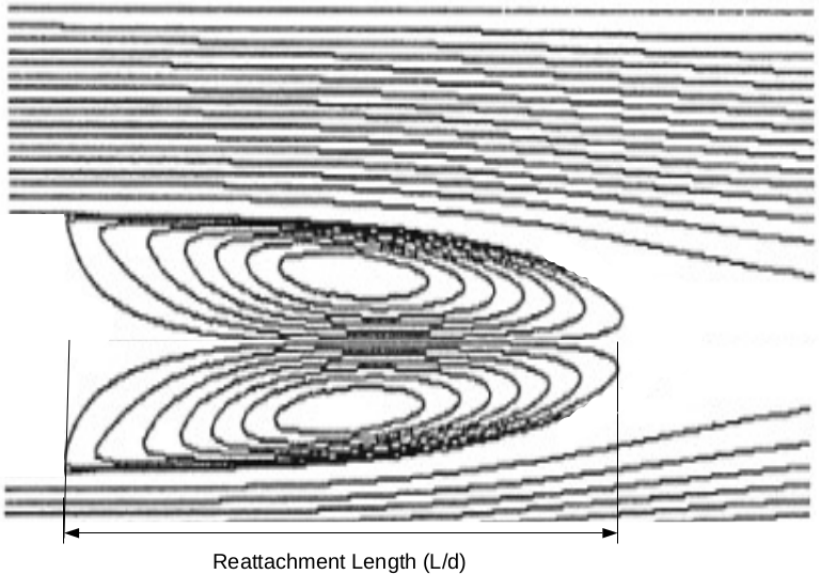

Figure 6 – Reattachment Length of vortex shedding.

RASHIDI et al. (2013) has reached wake lengths results for different porosities of the sheat, in which the cylinder was encased, and tested without the porous sheat. The second one was simulated as a solid cylinder, and a good agreement has been taken. BHATTACHARYYA; DHINAKARAN; KHALILI (2006) predicted wake-length as a function of Re at different Da. Wake Lengths for $Da = 10^{-6}$ were found to be in good agreement with those of solid cylinder. 1986 (1986) studied the evolution of the reattachment length and the velocity field of the steady-state flow around a solid cylinder, for Reynolds numbers of 20 and 40. Two attached vortices are formed behind the cylinder. Good agreement with the experimental results of the literature is obtained.

The present work validated the methodology comparing the reattachment length and the velocity field with the literature for solid and porous cylinder cited above. The next section will present the formulation of a convection problem of a solid and porous circle cylinder surrounded by a incompressible fluid flow.

3 MATHEMATICAL FORMULATION

3.1 Governing Equations

The mathematical formulation is presented in this section, in which the physical problem adjusts the governing equation of a general model of fluid flow to one through and surrounding a porous media. The approach uses the Brinkman-Forchheimer modification for the Darcy equation to porous media, handling as a single domain problem. Despite applying a set of equations for each region (open and porous domain), the Single Domain approach validates a set of equations for all points in the whole domain (BRETON; CALTAGIRONE; ARQUIS, 1991)(CORNELISSEN, 2016).

In the present work following assumptions are made:

•Two-dimensional, unsteady, laminar flow of an incompressible and viscous flow has been considered.

• The porous medium is isotropic, uniform and homogeneous.

• The porous cylinder is completely saturated with water.

• One-domain approach is used for governing equations.

• The diameter of porous cylinder is sufficiently larger than the characteristics radius of the pores.

Formulation of porous media problems using normalized variables can provide many advantages. The order of magnitude of the normalized variables is the same, and therefore the numerical round-off errors resulting from calculations with different orders of magnitude values are avoided (VERSTEEG; MALALASEKERA, 2007). Figure (7) shows the schematic numerical grid. The problem is formuled in a cartesian coordinates, 51x84 mesh points in the x and in the y direction respectivaly. Besides, dx and dy both are equal to 0,24. A finer grid distribution is imposed around 0 in and y coordinates.

The nondimensionalized variables are defined as follows:

$$x = \frac{\overline{x}}{d},\ y = \frac{\overline{y}}{d},\ u = \frac{\overline{u}}{u_0},\ v = \frac{\overline{v}}{u_0},\ p = \frac{\overline{p}}{\rho u_0^2},\ t = \frac{\overline{t}}{t_c},\ c = \frac{\overline{c}}{c_0},$$

where $\overline{x}$ and $\overline{y}$ are spatial coordinates, and their respectively $\overline{u}$ and $\overline{v}$ velocity components, u_0 is the velocity of injection, d is the diameter of the cylinder, $\overline{p}$ is the pressure, t is the time, and c is the dimensionless concentration. The velocity of fluid in the porous media v is related by the free fluid velocity by the Dupuit–Forchheimer equation $v = \varepsilon V$, where ε is the porosity and V is the velocity in the free fluid region (NIELD; BEJAN, 2017). The governing equations for conservation of mass, momentum and concentration are given by equations:

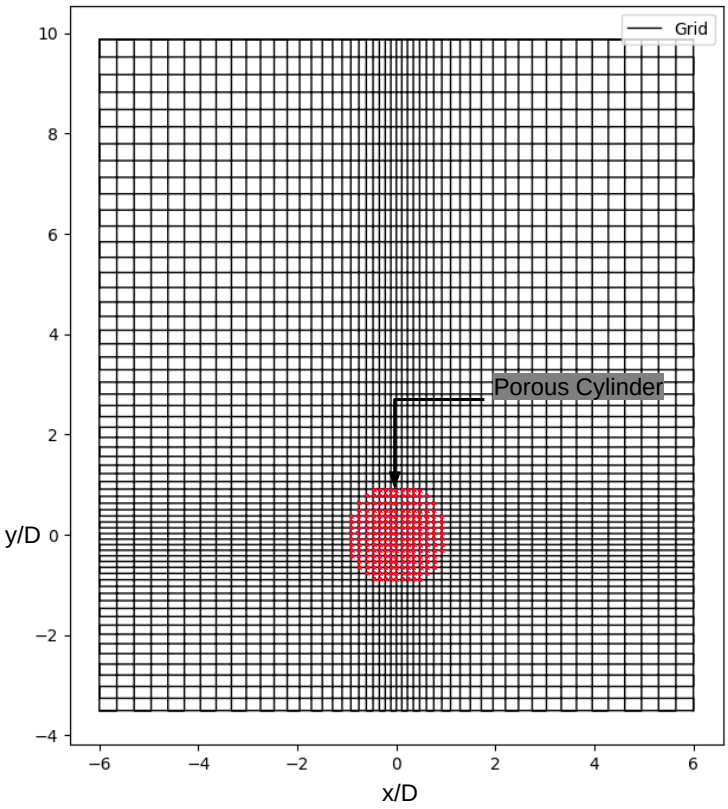

Figure 7 – Schematic mumerical grid.

$$\frac{1}{\beta}\frac{\partial p}{\partial \tau} + \frac{1}{\varepsilon}\frac{\partial u}{\partial x} + \frac{1}{\varepsilon}\frac{\partial v}{\partial y} = 0, \tag{13}$$

$$\frac{\partial u}{\partial \tau} + \frac{1}{\varepsilon}\frac{\partial (uu)}{\partial x} + \frac{1}{\varepsilon}\frac{\partial (vu)}{\partial y} = -\varepsilon\frac{\partial p}{\partial x} + \frac{1}{Re}\left(\frac{\partial^2 u}{\partial x^2} + \frac{\partial^2 u}{\partial y^2}\right) + \varepsilon B\Phi_x, \tag{14}$$

$$\frac{\partial v}{\partial \tau} + \frac{1}{\varepsilon}\frac{\partial (uv)}{\partial x} + \frac{1}{\varepsilon}\frac{\partial (vv)}{\partial y} = -\varepsilon\frac{\partial p}{\partial y} + \frac{1}{Re}\left(\frac{\partial^2 v}{\partial x^2} + \frac{\partial^2 v}{\partial y^2}\right) + \varepsilon B\Phi_y. \tag{15}$$

$$\frac{\partial (C)}{\partial \tau} + \frac{1}{\varepsilon}\frac{\partial (uC)}{\partial x} + \frac{1}{\varepsilon}\frac{\partial (vC)}{\partial y} = \frac{1}{ReSc}\left(\frac{\partial^2 C}{\partial x^2} + \frac{\partial^2 C}{\partial y^2}\right) \tag{16}$$

In the continuity equation, a time-dependent pressure term together with a multiplicative parameter nominated as artificial compressibility $1/\beta$. (SIIKONEN MM RAHMAN, 2001; CHORIN, 1997). The numerical procedure is performed until the pseudo-transient turns negligible, Eq.(13) (KWAK; KIRIS, 2011; CHANG; KWAK, 1984). The regions of porous media and fluid are controled by the parameters of Eqs. (14) and (15) as

$$B = \begin{cases} 0, & \text{outside porous media} \\ 1, & \text{inside porous media} \end{cases} \tag{17}$$

the condition $B = 0$ means that $Da \to \infty$ at the fluid region, and the porosity is defined as

$$\varepsilon = \begin{cases} 1, & \text{outside porous media} \\ 0 < \varepsilon_0 < 1, & \text{inside porous media} \end{cases} \tag{18}$$

The porous media is modeled by Darcy-forchheimer equation, where Φ is the internal frictional drag given by

$$\Phi_x = -\frac{u}{Re.Da} + \frac{c_f}{\sqrt{Da}} u\sqrt{u^2 + v^2}, \tag{19}$$

$$\Phi_y = -\frac{v}{Re.Da} + \frac{c_f}{\sqrt{Da}} v\sqrt{u^2 + v^2}, \tag{20}$$

in which Re is the Reynolds number of free flow, Da is the Darcy number defined as $Da = K/d^2$. The parameter c_f is a dimensionless form-drag constant. c_f is the Forchheimer coefficient and to a cylinder filled with homogeneous spheres the expression adopted by BOVAND et al., gived by Be. 10.

3.1.1 Boundary conditions

The initial and boundary conditions for the equations are specified as
Initial conditions ($\tau = 0$):

$$u(x, y) = 0, \quad v(x, y) = v_i \quad \text{everywhere} \tag{21}$$

$$C(x, y) = \begin{cases} C_\infty, & \text{outside porous media} \\ C_p, & \text{inside porous media} \end{cases} \tag{22}$$

in which C_p is the concentration of the porous media.

The boundary conditions ($\tau > 0$):

$$u(x, -L_y) = 0, \quad v(x, -L_y) = v_i, \text{at the inlet boundary}, \tag{23}$$

$$u(x, L_y) = 0, \quad \left.\frac{\partial v}{\partial y}\right|_{(x, L_y)} = 0, \quad \text{at the outlet bondary}, \tag{24}$$

$$u(-L_x, y) = 0, \quad \left.\frac{\partial v}{\partial x}\right|_{(-L_x, y)} = 0, \quad \text{in the left side}, \tag{25}$$

$$u(L_x, y) = 0, \quad \left.\frac{\partial v}{\partial x}\right|_{(L_x, y)} = 0, \quad \text{in the right side}, \tag{26}$$

in which V_i is velocity of injection. The center of the cylinder is located at the origin of the Cartesian system as shown in Fig. (7). Thus the domain has length $2L_x$ and the height measuring $L_y = |2,5(-L_y)|$.

3.2 Finite Volume Method

The finite volume method (FVM) is a widely used numerical technique. In this method, the domain is divided up in to discrete control volumes, where each node $P(i,j)$ is surrounded by a control volume. The boundaries of control volumes are positioned midway between adjacent nodes. Each control volume has width Δx and height Δy. As a consequence, the physical boundaries conincide with the control volume boundaries, as shown in the Fig.(8). Each point $P(i,j)$ is bounded by neighboring points placed at the

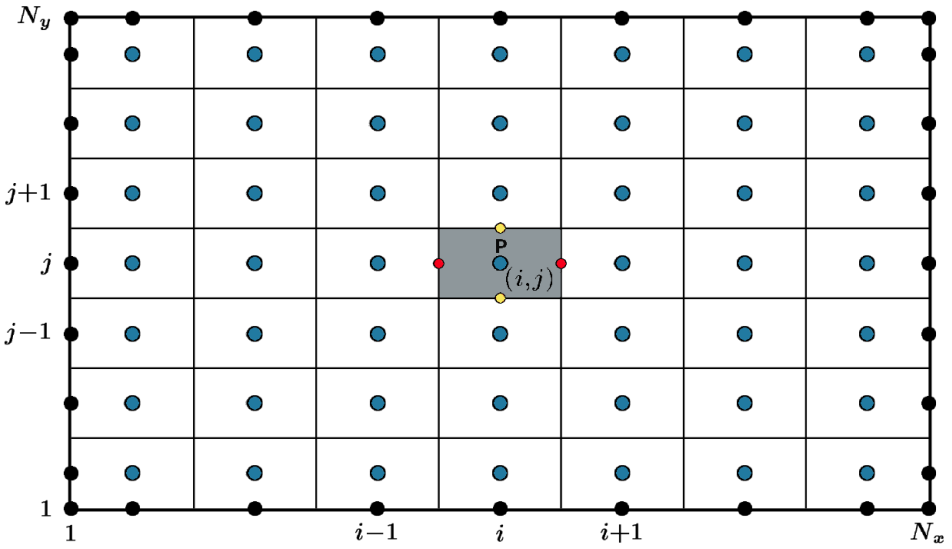

Figure 8 – Discrete control volumes inside of the domain

interface between the two adjacent volumes named $n(i, j + \frac{1}{2})$, $s(i, j - \frac{1}{2})$ for North and South, $w(i - \frac{1}{2}, j)$, $e(i + \frac{1}{2}, j)$ for East and West. Similarly, points placed at the center of the neighboring control volumes are definded as $N(i, j + 1)$, $S(i, j - 1)$ for North and South, $W(i - 1, j)$, $E(i + 1, j)$ for East and West, see Fig. (9). In addition, the distances between the points W and P, and between points P and E, are identified by δx_w and δx_e, respectively. Similarly, the distances between the points N and P, and between points P and S, are identified by δy_n and δy_s, respectively.

3.2.0.1 Integration of equations

The main feature of FVM is that the conservations equations are integrated over the control volume based on the Fig. (9) (BLAZEK, 2001; CHAPRA S.; CANALE, 2011). Thus the continuity equation, Eq. (13) is integrated over the control volume as

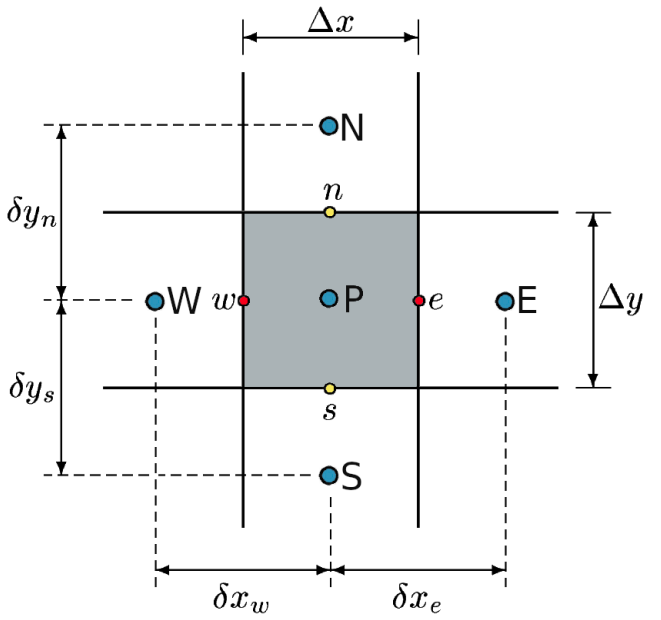

Figure 9 – Schematic figure of single control volume and neighboring points.

$$\frac{1}{\beta\Delta\tau}\int_{\tau}^{\tau+\Delta\tau}\frac{\partial p}{\partial\tau}\Delta\Omega d\tau+\int_{s}^{n}\int_{w}^{e}\frac{1}{\varepsilon}\frac{\partial u}{\partial x}dxdy+\int_{s}^{n}\int_{w}^{e}\frac{1}{\varepsilon}\frac{\partial v}{\partial y}dxdy=0, \tag{27}$$

resulting in

$$\frac{\varepsilon}{\beta}\frac{\Delta\Omega}{\Delta\tau}(p_P^{\nu+1}-p_P^{\nu})+\Delta y(u_e-u_w)+\Delta x(u_n-u_s)=0, \tag{28}$$

in which $\Delta\Omega=\Delta x\Delta y$ is the volume because $\Delta z=1$ for simplicity.

Similarly, the momentum conservation, Eq.(14), in x-direction is integrated

$$\begin{aligned}\frac{1}{\beta\Delta\tau}\int_{\tau}^{\tau+\Delta\tau}\frac{\partial u}{\partial\tau}\Delta\Omega d\tau+\int_{s}^{n}\int_{w}^{e}\frac{1}{\varepsilon}\frac{\partial(uu)}{\partial x}dxdy+\int_{s}^{n}\int_{w}^{e}\frac{1}{\varepsilon}\frac{\partial(vu)}{\partial y}dxdy=\\ -\int_{s}^{n}\int_{w}^{e}\varepsilon\frac{\partial p}{\partial x}dxdy+\int_{s}^{n}\int_{w}^{e}\frac{\partial}{\partial x}\left(\frac{\varepsilon}{Re}\frac{\partial u}{\partial x}\right)dxdy+\\ \int_{s}^{n}\int_{w}^{e}\frac{\partial}{\partial y}\left(\frac{\varepsilon}{Re}\frac{\partial u}{\partial y}\right)dxdy-\int_{s}^{n}\int_{w}^{e}\varepsilon B\Phi_x dxdy,\end{aligned}$$

resulting in

$$\begin{aligned}\frac{\Delta\Omega}{\Delta\tau}(u_P^{\nu+1}-u_P^{\nu})+F_e u_e-F_w u_w+F_n u_n-F_s u_s=-\varepsilon\frac{p_e-p_w}{\Delta x}\Delta\Omega+\\ D_e(u_E-u_P)-D_w(u_P+u_W)+D_n(u_N-u_P)-D_s(u_P+u_S)+\varepsilon B\Phi_x\Delta\Omega\end{aligned} \tag{29}$$

in which $F_f=A_f u_f/\varepsilon$, $D_f=\varepsilon A_f/(Re\ \delta x_f)$ and the subscript f could be n, s, e, w.

In the same way, the momentum conservation equation in y-direction is integrated

over the control volume

$$\frac{1}{\Delta\tau}\int_{\tau}^{t+\Delta\tau}\frac{\partial v}{\partial\tau}\Delta\Omega d\tau+\int_{s}^{n}\int_{w}^{e}\frac{1}{\varepsilon}\frac{\partial(uv)}{\partial x}dxdy+\int_{s}^{n}\int_{w}^{e}\frac{1}{\varepsilon}\frac{\partial(vv)}{\partial y}dxdy=$$
$$-\int_{s}^{n}\int_{w}^{e}\varepsilon\frac{\partial p}{\partial y}dxdy+\int_{s}^{n}\int_{w}^{e}\frac{\partial}{\partial x}\left(\frac{\varepsilon}{Re}\frac{\partial v}{\partial x}\right)dxdy+$$
$$\int_{s}^{n}\int_{w}^{e}\frac{\partial}{\partial y}\left(\frac{\varepsilon}{Re}\frac{\partial v}{\partial y}\right)dxdy-\int_{s}^{n}\int_{w}^{e}\varepsilon B\Phi_{y},$$

resulting in

$$\frac{\Delta\Omega}{\Delta\tau}(v_P^{\nu+1}-v_P^{\nu})+F_e v_e-F_w v_w+F_n v_n-F_s v_s=-\varepsilon\frac{p_n-p_s}{\Delta y}\Delta\Omega+$$
$$D_e(v_E-v_P)-D_w(v_P+v_W)+D_n(v_N-v_P)-D_s(v_P+v_S)+\varepsilon B\Phi_y\Delta\Omega, \quad (30)$$

in which $F_f=A_f v_f/\varepsilon$, $D_f=\varepsilon A_f/(Re\ \delta y_f)$ and the subscript f could be n,s,e,w. The bouancy therm is defined as

$$F_g=\frac{1}{Sc}\left(1-\frac{1}{(C_n+C_s)/2}\right)$$

Sc is the Schimdt Number is used in order to determine the resistance of the flow by moving around a body at a certain speed. The dimensionless number as the ratio of momentum diffusivity and mass diffusivity: $Sc=\frac{\nu}{\sigma}$, σ is the diffusivity and ν is kinematic viscosity. The concentration conservation as a function of concentration is integrated

$$\frac{1}{\Delta\tau}\int_{\tau}^{t+\Delta\tau}\frac{\partial C}{\partial\tau}\Delta\Omega d\tau+\int_{s}^{n}\int_{w}^{e}\frac{1}{\varepsilon}\frac{\partial(uC)}{\partial x}dxdy+\int_{s}^{n}\int_{w}^{e}\frac{1}{\varepsilon}\frac{\partial(vC)}{\partial y}dxdy=$$
$$\int_{s}^{n}\int_{w}^{e}\frac{\partial}{\partial x}\left(\frac{1}{ReSc}\frac{\partial C}{\partial x}\right)dxdy+\int_{s}^{n}\int_{w}^{e}\frac{\partial}{\partial y}\left(\frac{1}{ReSc}\frac{\partial C}{\partial y}\right)dxdy \quad (31)$$

resulting in

$$\frac{\Delta\Omega}{\Delta\tau}(C_P^{\nu+1}-C_P^{\nu})+F_e C_e-F_w C_w+F_n C_n-F_s C_s=$$
$$D_e(C_E-C_P)-D_w(C_P+C_W)+D_n(C_N-C_P)-D_s(C_P+C_S) \quad (32)$$

in which $F_f=A_f v_f/\varepsilon$ and $D_f=A_f/(ReSc\ \delta x_f)$

After the integration of equations by finite volume, a system of sparse linear given by Eqs. (29), (30) and (32) is generated. However, the fluxes of the transported property through control volume faces must be properly calculated. For example, the flux coming out a control volume across a certain face must be equal to the flux coming in of the adjacent control volume through the same face (VERSTEEG H. K.; MALALASEKERA, 2007). Thus, the flux through a common face must be modeled. In the present work, the QUICK-scheme

will be used.

3.2.0.2 QUICK scheme

Quadratic Upstream Interpolation for Convective Kinematics, named QUICK-scheme is one of the methods highly used to solve convection problems, based on a conservative control volume integral formulation (LEONARD, 1979). This safety is guaranteed by the good accuracy due to third-order spatial truncation error and first-order accurate in time. This method considers the weighted quadratic interpolation of three points upstream for the values of the cell face (VERSTEEG; MALALASEKERA, 2007). Figure (10) shown the schematic grid for one-dimensional domain.

The choice of storing the properties (u, v, p and C) at the geometrical centre of the control volume usually leads to non-physical oscillations and the difficulties in obtaining a converged solution (RODI; MAJUMDAR; SCHöNUNG, 1989). Therefore the velocities must be estimated a long cell face (w and e). Using some assumed interpolation profile, u_w and u_e can be formulated by a relationship of the form $u_f = f(u_{NB})$, in which NB denotes the u avalued at the neighboring nodes. To ensure coupling between the pressure

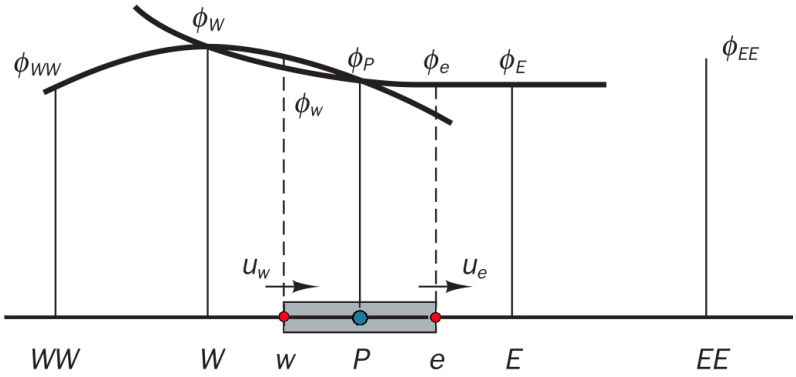

Figure 10 – Quick scheme interpolation for properties evaluated at the cell face

and velocity field a second and third gridies, which are staggered in the x-direction and y-direction relatives to the original grid, are used for the velocity components u and v, with the pressure being calculated in the original grid, as shown in Fig (11). The temperature is also evalueated at the original grid. Note that, the u and v velocity components area evalued, respectively, by red and yellow points, as shown in the Fig. (11). This procedure is known as staggered grid. Thus, the Quick scheme is used and the velocity at the volume interfaces are calculed by a quadractic interpolation in upwind scheme:

$$u_w = \frac{6}{8}u_W + \frac{3}{8}u_P - \frac{1}{8}u_{WW} \tag{33}$$

$$u_e = \frac{6}{8}u_P + \frac{3}{8}u_E - \frac{1}{8}u_W \tag{34}$$

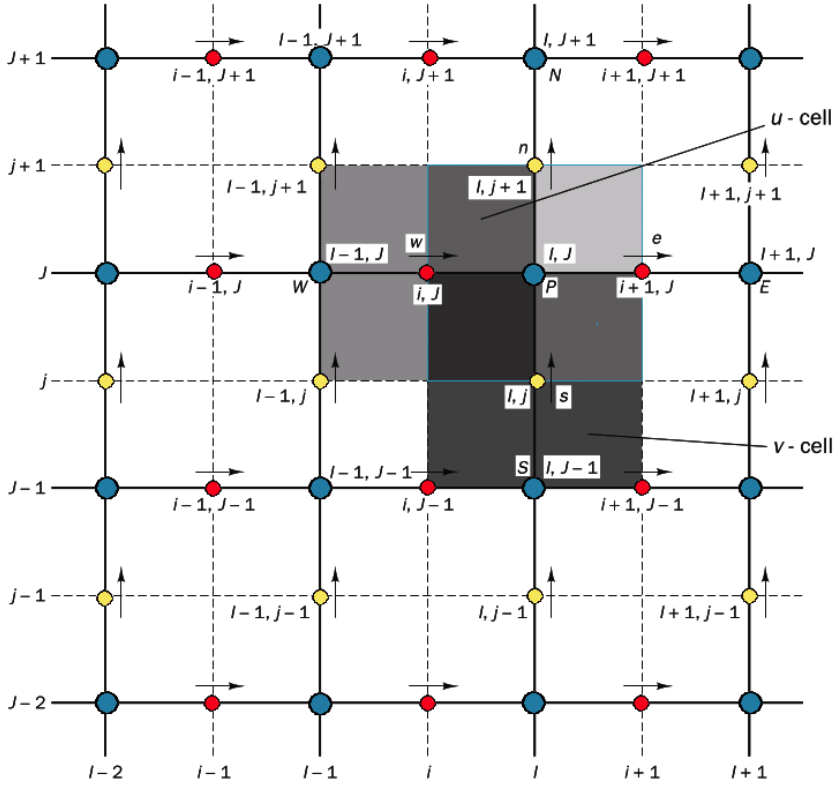

Figure 11 – Staggered grid: blue points are original grid, red and yellow points stands to local of evaluation of the u and v velocities components, respectively.

$$u_s = \frac{6}{8}u_S + \frac{3}{8}u_P - \frac{1}{8}u_{SS} \tag{35}$$

$$u_n = \frac{6}{8}u_P + \frac{3}{8}u_N - \frac{1}{8}u_S \tag{36}$$

for $u_w > 0$, $u_e > 0$, $u_s > 0$ and $u_n > 0$.

$$u_w = \frac{6}{8}u_P + \frac{3}{8}u_W - \frac{1}{8}u_E \tag{37}$$

$$u_e = \frac{6}{8}u_E + \frac{3}{8}u_P - \frac{1}{8}u_{EE} \tag{38}$$

$$u_s = \frac{6}{8}u_P + \frac{3}{8}u_S - \frac{1}{8}u_N \tag{39}$$

$$u_n = \frac{6}{8}u_N + \frac{3}{8}u_P - \frac{1}{8}u_{NN} \tag{40}$$

for $u_w < 0$, $u_e < 0$, $u_s < 0$ and $u_n < 0$. Replacing Eqs.(33) to (40) in Eq.(29) results in

$$\frac{\Delta\Omega}{\Delta\tau}(u_P^{\nu+1}-u_P^{\nu})+a_P u_P=-\varepsilon\frac{p_e-p_w}{\Delta x}\Delta\Omega+a_W u_W+a_E u_E+a_S u_S+ \\ a_N u_N+a_{WW}u_{WW}+a_{SS}u_{SS}+a_{EE}u_{EE}+a_{NN}u_{NN}+\varepsilon B\Phi_x\Delta\Omega \quad (41)$$

$$a_P=a_W+a_E+a_S+a_N+a_{WW}+a_{EE}+a_{SS}+a_{NN}+F_e-F_w+Fn-F_s \quad (42)$$

$$a_W=D_w+\frac{6}{8}\alpha_w F_w+\frac{1}{8}\alpha_e F_e+\frac{3}{8}(1-\alpha_w)F_w \quad (43)$$

$$a_E=D_e-\frac{3}{8}\alpha_e F_e-\frac{6}{8}(1-\alpha_e)F_e-\frac{1}{8}(1-\alpha_w)F_w \quad (44)$$

$$a_S=D_s-\frac{6}{8}\alpha_s F_s+\frac{1}{8}\alpha_n F_n-\frac{3}{8}(1-\alpha_s)F_s \quad (45)$$

$$a_N=D_n-\frac{3}{8}\alpha_n F_n-\frac{6}{8}(1-\alpha_n)F_n-\frac{1}{8}(1-\alpha_s)F_s \quad (46)$$

$$a_{WW}=-\frac{1}{8}F_w \quad (47)$$

$$a_{EE}=\frac{1}{8}(1-\alpha_e)F_e \quad (48)$$

$$a_{SS}=-\frac{1}{8}F_s \quad (49)$$

$$a_{NN}=\frac{1}{8}(1-\alpha_n)F_n \quad (50)$$

in which

$$\alpha_w=1 \quad \text{for} \quad F_w>0 \quad \text{and} \quad \alpha_e=1 \quad F_e>0$$
$$\alpha_w=0 \quad \text{for} \quad F_w<0 \quad \text{and} \quad \alpha_e=0 \quad F_e<0$$

$$\alpha_s=1 \quad \text{for} \quad F_s>0 \quad \text{and} \quad \alpha_n=1 \quad F_n>0$$
$$\alpha_s=0 \quad \text{for} \quad F_s<0 \quad \text{and} \quad \alpha_n=0 \quad F_n<0$$

Thus, the same procedure is performed for momentum conservation in y-direction (Eq.

(30)) resulting in

$$\frac{\Delta\Omega}{\Delta\tau}(v_P^{\nu+1} - v_P^{\nu}) + a_P v_P = -\varepsilon\frac{p_n - p_s}{\Delta x}\Delta\Omega + a_W u_W + a_E u_E + a_S u_S + a_N u_N + a_{WW} u_{WW} + a_{SS} u_{SS} + a_{EE} u_{EE} + a_{NN} u_{NN} + (\varepsilon B\Phi_y + F_g)\Delta\Omega \quad (51)$$

Finaly, the solution of Eqs. (28), (29), (30) and (32) as will be shown in the next section.

4 MATERIALS AND METHODS

This work presents a simple case for external flows around the cylindrical porous media. The set of equations (13) to (16) are solved in its discretization form given by Eqs. (29), (30) and (32). The pressure field is solved by artifical compressibility method. Artificial compressibility is introduced by adding a time derivative term for pressure to the continuity Eq. (13). Mathematically, this means that pseudo-waves are introduced into the incompressible flow field as a medium to distribute the pressure. Physically, the objective is maintaining incompressibility during iterative processes for obtaining solutions at each time level, i.e., when $\beta^{-1}\partial p/\partial \tau << 1$, the continuity equation is satisfied at each time step in Eq. (13). More details about artificial compressibility method can be found in KWAK; KIRIS, 2011. The transient incompressible solution is obtained. Thus an iterative method is employed at each time step, which is equivalent to solving the governing equations for steady state at each time level. The sequence of operations of the numerical procedure which employs the algorithm is given by

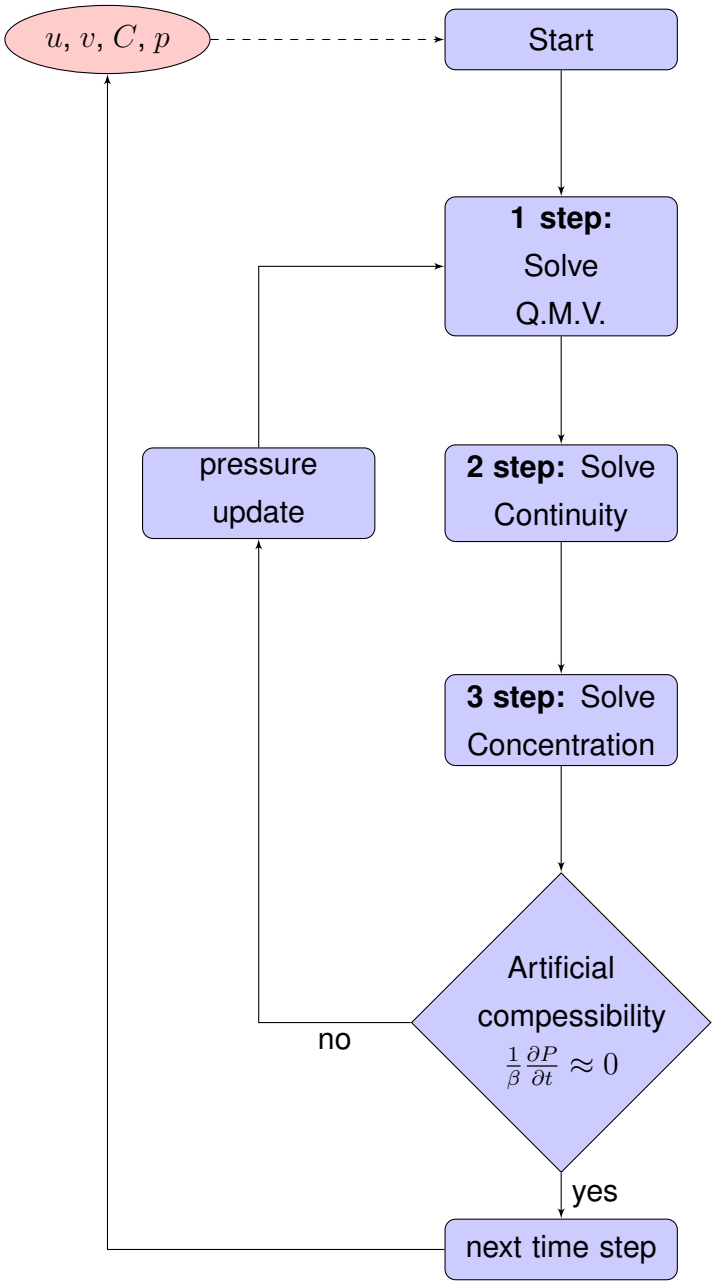
u, v, C, p
Start
1 step: Solve Q.M.V.
2 step: Solve Continuity
3 step: Solve Concentration
Artificial compessibility $\frac{1}{\beta}\frac{\partial P}{\partial t} \approx 0$
no
pressure update
yes
next time step

5 RESULTS AND DISCUSSION

The results and discussions are shown in this section. The porous cylinder is placed in an environment at forced flow. At the bottom of domain, the fluid is injected with constant velocity $U = 1.0$. The present flow field is governed by four parameters namely, Reynolds number (Re), Schmidt Number (Sc), Porosity (ε) and Darcy number (Da).

At the bottom of domain, the fluid is injected with constant velocity $U = 1.0$. The present flow field is governed by four parameters namely, Reynolds number (Re), Schmidt Number (Sc), Porosity (ε) and Darcy number (Da). First, these parameters were varied in the way to analyze a laminar flow behavior around a solid's circular cylinder aimed to validate the method. We have also compared our results of wake length with DENNIS; CHANG (1970), D'ALESSIO; DENNIS (D'ALESSIO; DENNIS) BHATTACHARYYA; DHINAKARAN; KHALILI (2006), and BRAZA; CHASSAING; MINH (1986), as showed in Fig. 12. Our results are in a good agreement with the literature, thus they behave with the described in the theory, L/d growing proportionaly with the Re.

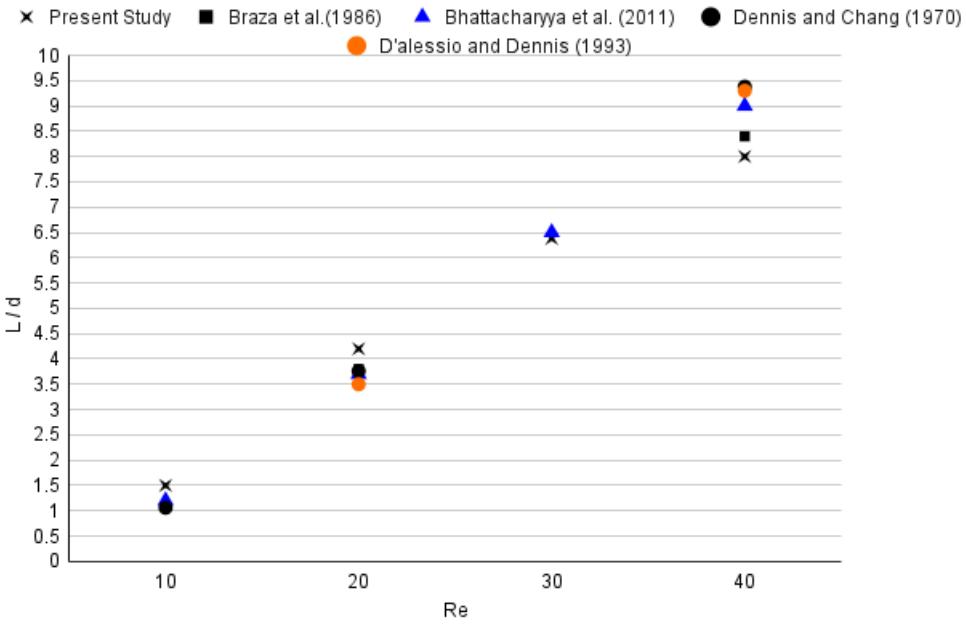

Figure 12 – Length of Wake for differents Re.

Fig.13 shows the development of streamlines around a solid circular cylinder according to Reynolds Number, which velocity in the cylinder boundaries is zero. It is a classic case of convection around cylinders used to validate the present methodology. After a initial transition, the vortex shedding presents a steady and symmetrical development for Reynolds number below 40. The length of wake of the vortex is analized in streamlines figures. The transient solution allows observing all described regimes in Fig. (5). Initially, the flow is at low speed and the streamline is symmetrical around the cylinder, as shown in Fig.(13-a).

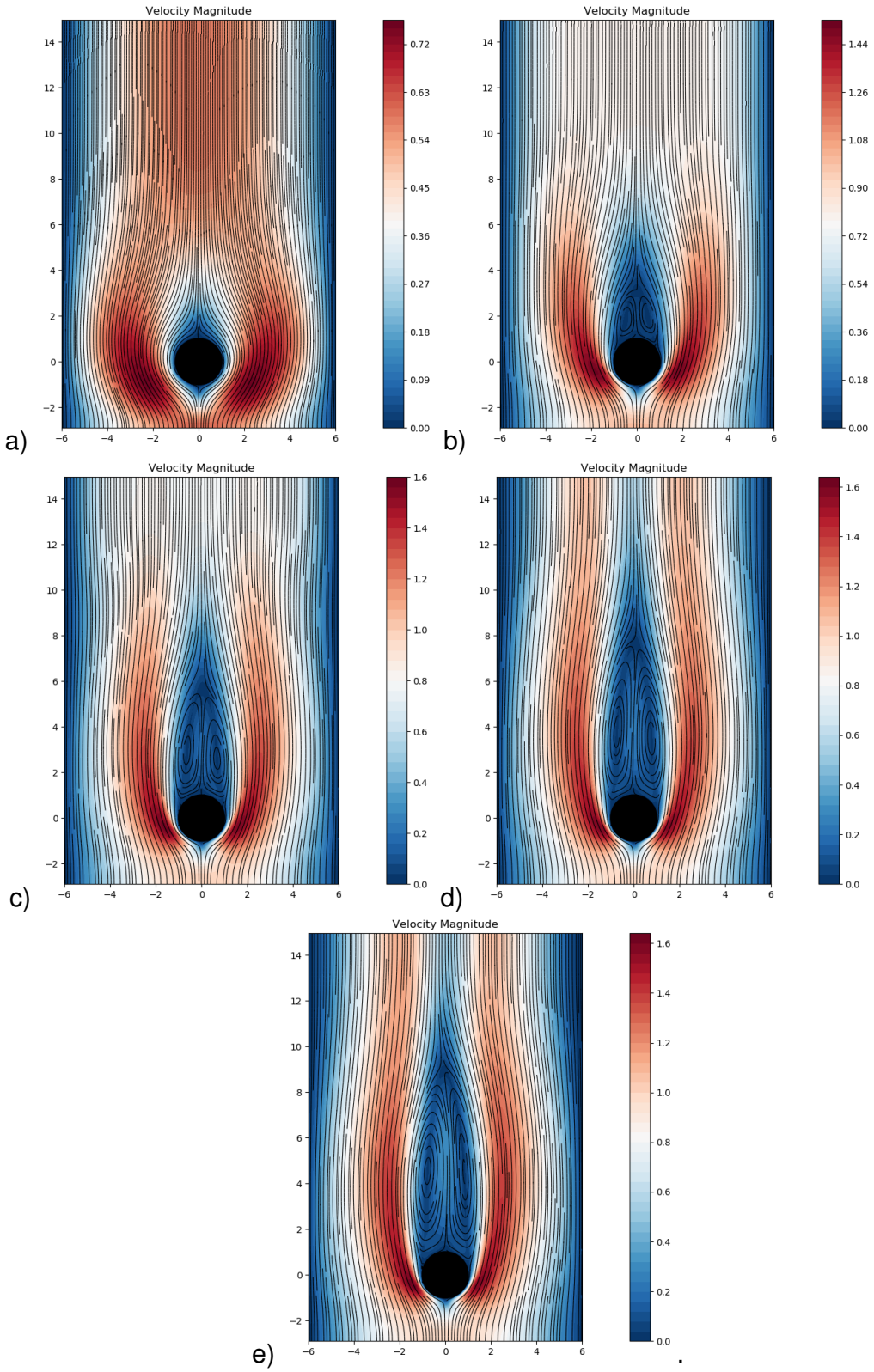

Figure 13 – Streamlines around a rigid cylinder over diferents Re. a) Re = 1, b) Re= 10, c) Re=20, d) Re = 30 and e) Re = 40.

Afterwards, as the Re increases, a pair of vortices is formed and starts to increase with Re, as shown in (13b,c,d and e). The periodic pattern of the vortices is modified as the parameters of the porous media (ε and Da) change. Fig. 14 shows the decrease of the

vortices shedding proportionally as the Da enhances.

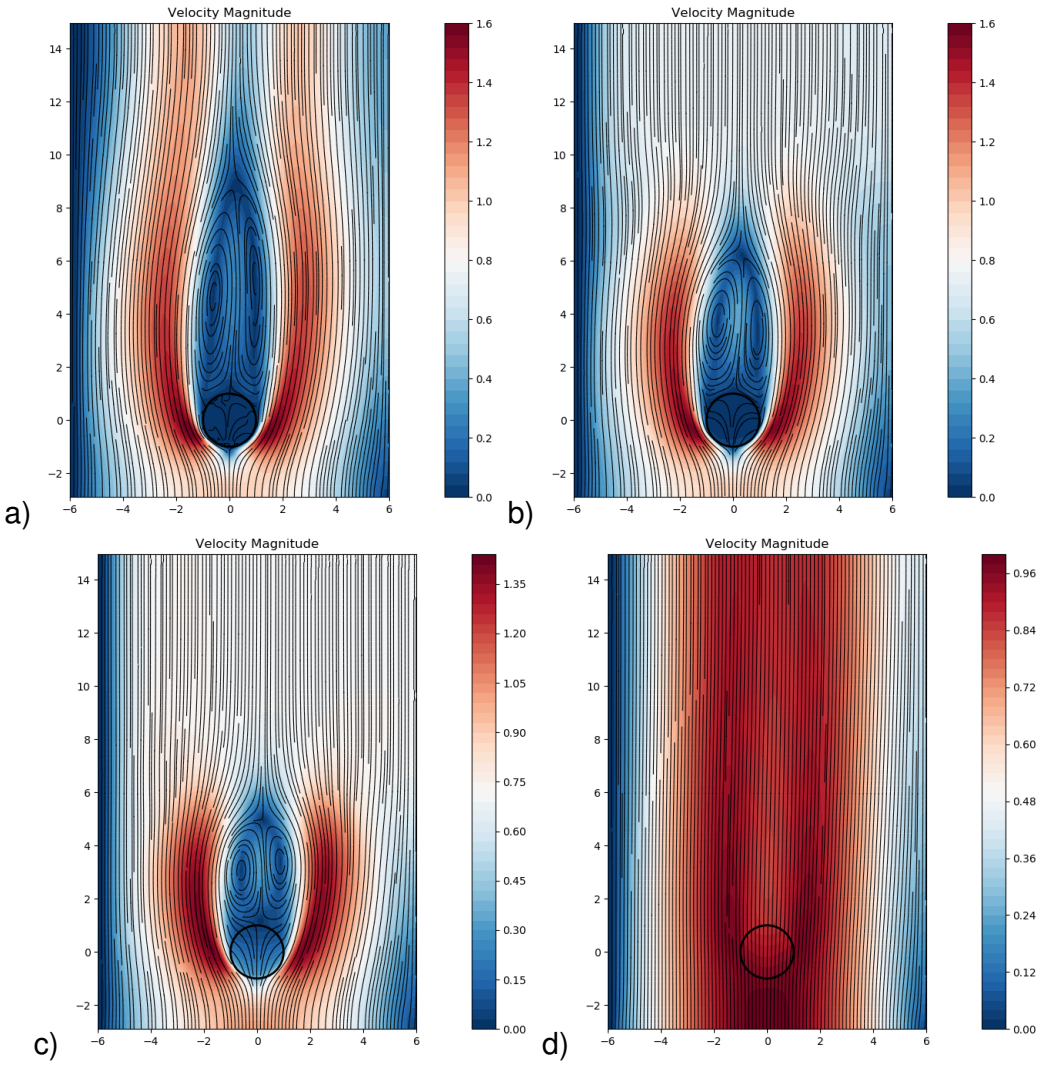

Figure 14 – Streamlines for Re = 30 and differents Da and ε. a)Da = 1x10^{-6}, ε = 0,693, b) Da = 1x10^{-3}, ε = 0,977, c) Da = 1x10^{-2}, ε = 0,993. and d) Da = 1, ε= 1.

For the porous cylinder case, the strength of the vortices are reduced in comparison with the solid cylinder. The vortices streamlines are only externally when a solid cylinder is considered. However, for porous cylinder cases, vorticity diffuses into both external and internal flow fields in the porous cylinder.

From the Fig.15, it is evident that the streamlines pattern are nearly the same as that of solid cylinder for Da = 1x10^{-6} for the range of Reynolds number considered and compared with the previews literature (Re=10, 20, 30 and 40). Even though the void volume is 62.9% of the total volume (ε = 0.629), at Da = 1x10^{-6} the porous cylinder behaves like a impermeable cylinder. The penetration through the cylinder is very small.

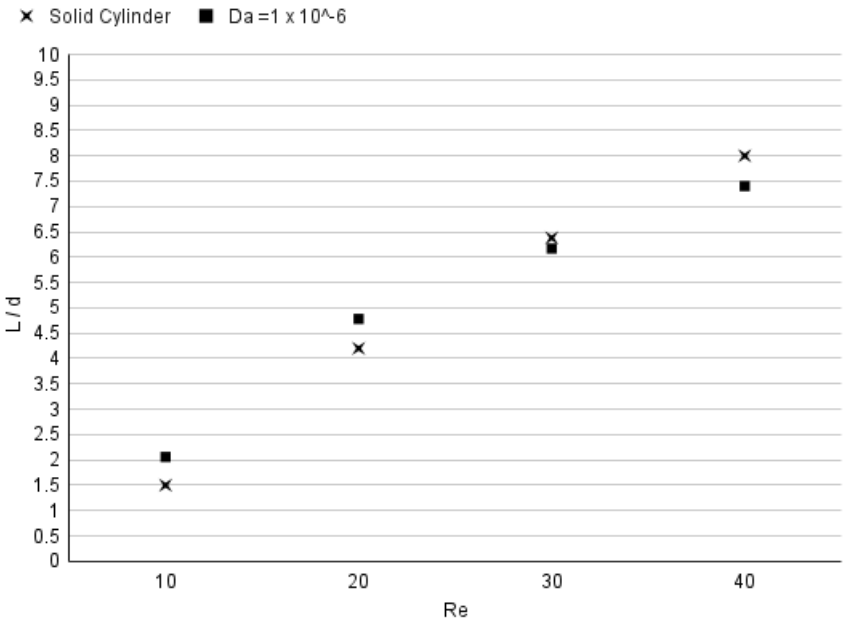

Figure 15 – Comparision of length of Wake of Solid Cylinder and Porous Cylinder (Da = 1 x10^{-6}) for diferents Re.

The Transient velocity pattern in different Re and Da is shown in Fig. 16. The vortices contour is compared from low Reynolds Numbers to highest ones, and from solid cylinder to porous cylinder. In addition to the decrease in the size of the vortices with the proportional increase in porosity, the delay in creating the vortices is evident in the transient development. The streamlines easily penetrate the porous region when Darcy number is high.

Re = 30, Solid Cylinder

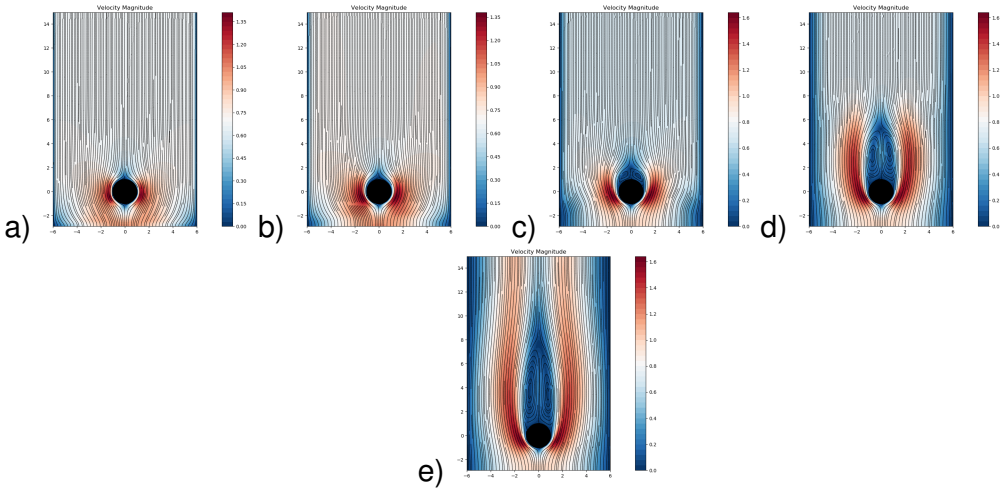

Re = 30, Da = 1x10^{-3}

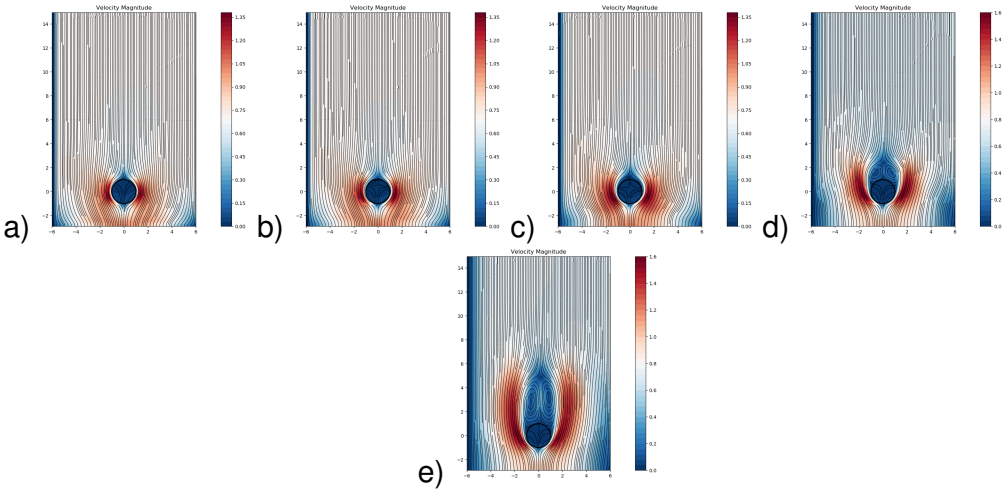

Re = 100 Solid Cylinder

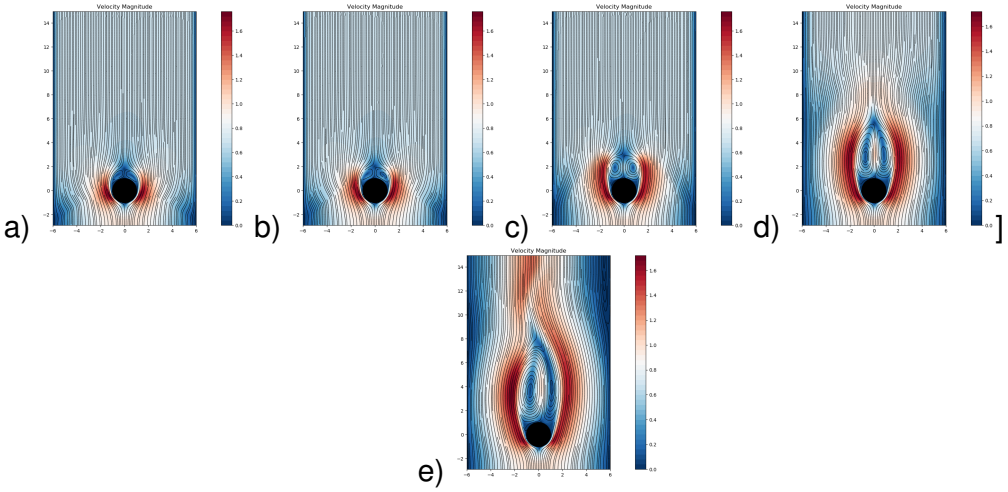

Re = 100, Da = 1x10^{-3}

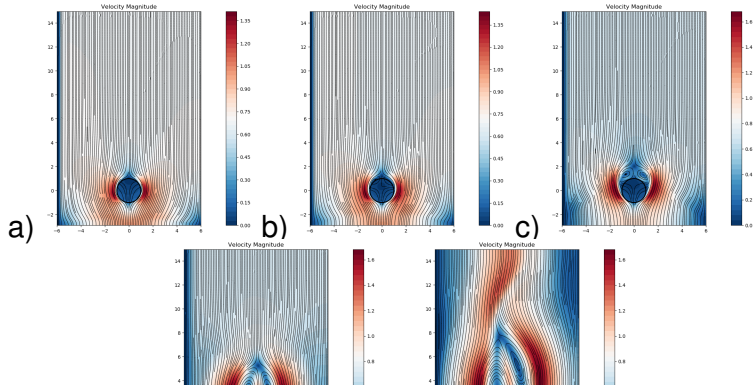

The transient development of concentration inside and around the porous cylinder is shown in Fig. 17 for Sc = 100 at differents dimensionless times 50, 100, 200 and 300, and different permeabilities (Da). Fluid flow forms two symmetric plume structures downstream, the porous region wastes more than 60% of the concentration at t= 100 for Da = 1x10^{-2} and Re = 30 . The region of zero concentration at the rear end of the cylinder ceases to exist at t =300 for Da = 1x10^{-2}. During the Re = 30 case, the transient concentration presents waste of around 10% content inside the porous cylinder at t = 300 for Da = 1x10^{-3}, and minimum waste for Da = 1x10^{-6} at the same time.

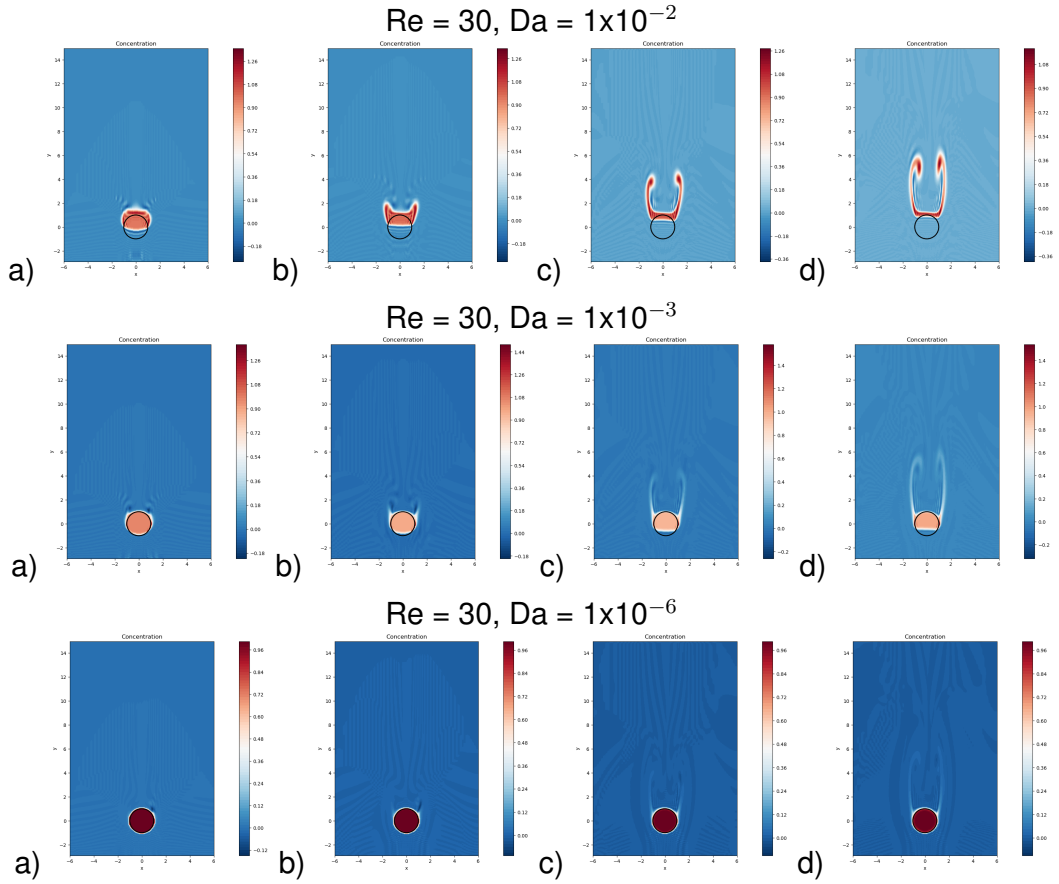

Figure 17 – Concentration for differents Da with Re = 30. a) t=50, b) t= 100, c) t = 200 and d) t= 300.

The transient development of concentration, for Re = 100, inside and around the porous cylinder is shown in Fig. 18 for Sc = 100 at differents dimensionless times 50, 100, 200 and 300, and different permeabilities (Da). Due to the strong convection of the fluid, it forms two symmetric plume structures downstream, the porous region wastes more than 95% of the concentration already at t= 100 for Da = 1x10^{-2}. The region of almost zero concentration at the rear end of the cylinder ceases to exist at t =100 for Da = 1x10^{-2} for Re = 100. Comparing with the Re = 30 case, during the transient of porous cylinder with Re = 100 case, the transient concentration presents waste of around 10% content inside the porous cylinder already at t = 100 for Da = 1x10^{-3}, but minimum waste for Da = 1x10^{-6}

at the same time.

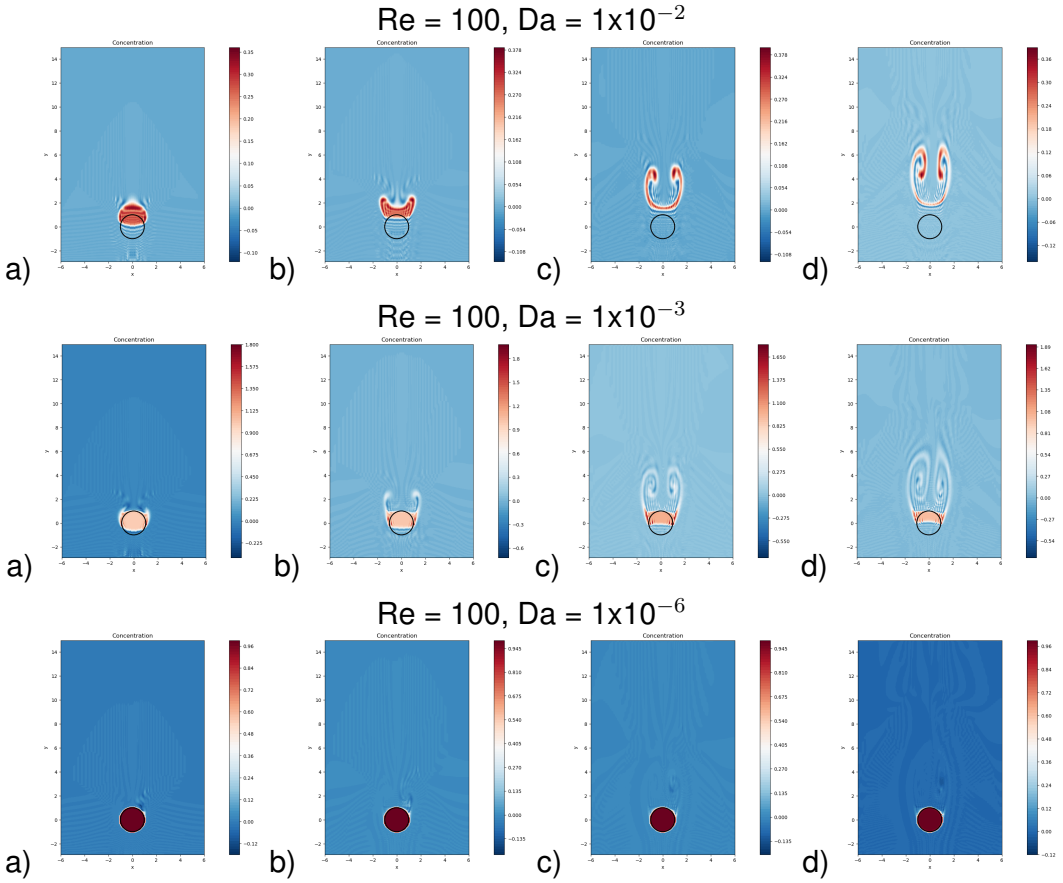

Figure 18 – Streamlines for Da= 1x10^{-2}, Da= 1x10^{-3}, Da= 1x10^{-6} and Re= 100 at various non-dimensional time. a) t=50, b) t= 100, c) t = 200 and d) t= 300.

For Re = 20, Da = 1x10^{-2} and ε = 0.993 case, it was investigated the length of tail of concentration called plume. Then, it was compared with BHATTACHARYYA; DHINAKARAN; KHALILI 2006, both Sc = 600. It was analyzed at five different non-dimensional times t = 10, 50, 100, and 150, as it is shown in Figure 19. The height of the domain was increased for better measurement of the concentration plume. The two symmetric plumes, created at t=10, start to become nonsymmetric at t=50 and join together to form a single-tail-like structure, at time t = 100. At time 100, the long and thick plume is formed downstream of the cylinder, with decreasing concentration at the outer edge. The length of the concentration tail is a bit shorter compared to the solution obtained by BHATTACHARYYA; DHINAKARAN; KHALILI (2006), but thicker and wavy.

It is important to know the dimensions of the plume to know the path that concentration will take. In the drying of grains, it is relevant to know the paths of the moisture removed from the grains to a better projection of the moisture removal equipment.

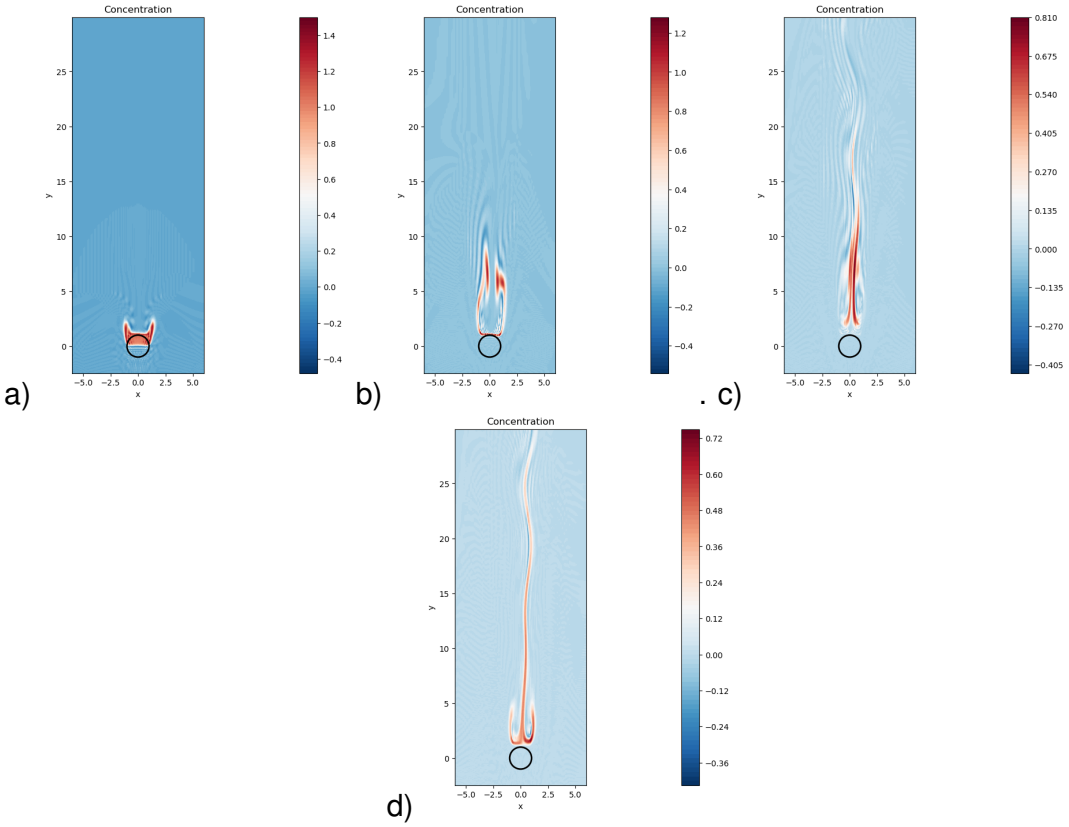

Figure 19 – Transient of Concentration for Re = 20, Sc=600 and Da = 1x10^{-2}. a) t = 10, b) t= 50, c) t=100, and d) t = 150.

6 CONCLUSION

A numerical study of velocity and concentration field in and around solid and a permeable cylinder has been done through a single-domain approach. We discovered that the flow field remains steady for the range of Reynolds number considered ($1 \leq Re \leq 40$), presenting symmetric and non-symmetric behavior as Re rise. At last, with high Re (Re> 90), destruction of the symmetric pattern (von Kármán vortex street) could be reproduced by our study.

The effects of Darcy and Reynolds numbers were analyzed and compared with previous literature, and good agreements were obtained. The increase in the length of the vortices wake was verified with the increase of the Reynolds Number (Re) for both cylinders: porous and solid cylinders, as well as, the decrease of the length of vortices with the increase of permeability (Da).The analysis of the concentration plume was done for a better understanding of the wet path in grain drying. Also an important information to help determine the drying rate in future studies.

In future works, we intend to use the Single-Domain approach, adding properties of the elements that are part of the grain drying process to better describe this phenomenon. Therefore, to emphasize the discussion of physical processes that occur in the flow.

BIBLIOGRAPHY

AMPRATWUM, D. B. Heat and moisture transfer and exchange in bulk grain. **Digital Repository@ Iowa State University**, 1976.

ANDRADE, E. T. d. et al. Determinação de propriedades térmicas de grãos de milho. **Ciência e Agrotecnologia**, SciELO Brasil, v. 28, n. 3, p. 488–498, 2004.

ASAE, T. Density, specific gravity and mass moisture relationship of grain for storage. **American Society of Agricultural Engineers**, 1993.

ATANGANA, A. Chapter 2 - principle of groundwater flow. In: ATANGANA, A. (Ed.). **Fractional Operators with Constant and Variable Order with Application to Geo-Hydrology**. [S.l.]: Academic Press, 2018. p. 15 – 47.

BABER, K. Coupling free flow and flow in porous media in biological and technical applications: From a simple to a complex interface description. 2014.

BALA, B.; WOODS, J. Simulation of deep bed malt drying. **Journal of Agricultural Engineering Research**, Elsevier, v. 30, p. 235–244, 1984.

BALA, B. K. **Drying and Storage of Cereal Grains**. [S.l.: s.n.], 2017. ISBN 9781119124238.

BALA, B. K.; BALA, B. **Drying and storage of cereal grains**. [S.l.]: Wiley Online Library, 1997.

BEAR, J. **Physical principles of water percolation and seepage**. [S.l.], 1968.

BEAVERS, G. S.; JOSEPH, D. D. Boundary conditions at a naturally permeable wall. **Journal of fluid mechanics**, Cambridge University Press, v. 30, n. 1, p. 197–207, 1967.

BECK, J. L. Convection in a box of porous material saturated with fluid. **The Physics of Fluids**, American Institute of Physics, v. 15, n. 8, p. 1377–1383, 1972.

BECKERMANN, C.; VISKANTA, R.; RAMADHYANI, S. Natural convection in vertical enclosures containing simultaneously fluid and porous layers. **Journal of Fluid Mechanics**, Cambridge University Press, v. 186, p. 257–284, 1988.

BEJAN A.; KRAUS, A. **Heat transfer handbook. Vol.1**. [S.l.]: John Wiley and Sons, 2003.

BHATTACHARYYA, S.; DHINAKARAN, S.; KHALILI, A. Fluid motion around and through a porous cylinder. **Chemical Engineering Science**, Elsevier, v. 61, n. 13, p. 4451–4461, 2006.

BHATTACHARYYA, S.; SINGH, A. Reduction in drag and vortex shedding frequency through porous sheath around a circular cylinder. **International journal for numerical methods in fluids**, Wiley Online Library, v. 65, n. 6, p. 683–698, 2011.

BLAZEK, J. **Computational Fluid Dynamics: Principles and Applications**. [S.l.]: ELSEVIER, 2001. 37 p.

BOVAND, M. et al. Control of wake and vortex shedding behind a porous circular obstacle by exerting an external magnetic field. **Journal of Magnetism and Magnetic Materials**, Elsevier, v. 385, p. 198–206, 2015.

BRAZA, M.; CHASSAING, P.; MINH, H. H. Numerical study and physical analysis of the pressure and velocity fields in the near wake of a circular cylinder. **Journal of fluid mechanics**, Cambridge University Press, v. 165, p. 79–130, 1986.

BRETON, P. L.; CALTAGIRONE, J.; ARQUIS, E. Natural convection in a square cavity with thin porous layers on its vertical walls. 1991.

BRINKMAN, H. A calculation of the viscous force exerted by a flowing fluid on a dense swarm of particles. **Flow, Turbulence and Combustion**, Springer, v. 1, n. 1, p. 27, 1949.

BROOKER D.B.; BAKKER-ARKEMA, F.; HALL, C. **Drying and storage of grains and oilseeds**. New York, USA: Van Nostrand Reinold, 1992. 265 p.

BRUNEAU, C.-H.; MORTAZAVI, I. Numerical modelling and passive flow control using porous media. **Computers & Fluids**, Elsevier, v. 37, n. 5, p. 488–498, 2008.

CAO, W.; NISHIYAMA, Y.; KOIDE, S. Physicochemical, mechanical and thermal properties of brown rice grain with various moisture contents. **International journal of food science & technology**, Wiley Online Library, v. 39, n. 9, p. 899–906, 2004.

CARRERA-RODRÍGUEZ, M. et al. Transient numerical study of the effect of ambient temperature on 2-d cereal grain storage in cylindrical silos. **Journal of stored products research**, Elsevier, v. 47, n. 2, p. 106–122, 2011.

CHANDESRIS, M.; JAMET, D. Boundary conditions at a planar fluid–porous interface for a poiseuille flow. **International Journal of Heat and Mass Transfer**, Elsevier, v. 49, n. 13-14, p. 2137–2150, 2006.

CHANG, J.; KWAK, D. On the method of pseudo compressibility for numerically solving incompressible flows. In: **22nd Aerospace Sciences Meeting**. [S.l.: s.n.], 1984. p. 252.

CHAPRA S.; CANALE, R. **Numerical Methods for Engineers**. [S.l.]: McGraw-Hill Companies Inc. New York., 2006.

____. **Numerical Methods for Engineers. 5 ed.** [S.l.]: McGraw-Hill Companies Inc. New York., 2011.

CHAUHAN, P.; CHOUDHURY, C.; GARG, H. Comparative performance of coriander dryer coupled to solar air heater and solar air-heater-cum-rockbed storage. **Applied thermal engineering**, Elsevier, v. 16, n. 6, p. 475–486, 1996.

CHEN, H.; WANG, X.-P. A one-domain approach for modeling and simulation of free fluid over a porous medium. **Journal of Computational Physics**, Elsevier, v. 259, p. 650–671, 2014.

CHIDYAGWAI, P.; RIVIÈRE, B. A two-grid method for coupled free flow with porous media flow. **Advances in Water Resources**, Elsevier, v. 34, n. 9, p. 1113–1123, 2011.

CHORIN, A. J. A numerical method for solving incompressible viscous flow problems. **Journal of computational physics**, Elsevier, v. 135, n. 2, p. 118–125, 1997.

CHUMA, Y. et al. Bulk physical and thermal properties of cereal grains as affected by moisture content. **Bulletin of Graduate School of Agriculture, Kyushu University**, Kyushu University, v. 26, n. 1, p. 57–70, 1981.

CORNELISSEN, P. **Coupled free-flow and porous media flow: a numerical and experimental investigation**. 2016. Dissertação (Mestrado), 2016.

COSTA, V. et al. Simulation of coupled flows in adjacent porous and open domains using acontrol-volume finite-element method. **Numerical Heat Transfer, Part A: Applications**, Taylor & Francis, v. 45, n. 7, p. 675–697, 2004.

D'ALESSIO, S.; DENNIS, S. A vorticity model for viscous flow past a cylinder. **Computers & fluids**, Elsevier, v. 23, n. 2, p. 279–293, 1994.

DENNIS, S.; CHANG, G.-Z. Numerical solutions for steady flow past a circular cylinder at reynolds numbers up to 100. **Journal of Fluid Mechanics**, Cambridge University Press, v. 42, n. 3, p. 471–489, 1970.

DESHPANDE, S.; BAL, S.; OJHA, T. Bulk thermal conductivity and diffusivity of soybean. **Journal of Food Processing and Preservation**, v. 20, p. 177 – 189, 05 2007.

ELGAMAL, R. et al. Development of a multi-scale model for deep-bed drying of rice. **Transactions of the ASABE**, American Society of Agricultural and Biological Engineers, v. 58, n. 3, p. 849–859, 2015.

ELGAMAL, R. A.; KISHK, S. S.; ELMASRY, G. M. Validation of cfd models for the deep-bed drying of rice using thermal imaging. **biosystems engineering**, Elsevier, v. 161, p. 135–144, 2017.

EMADI, B. R. .; ZARE, D. Cfd simulation of deep-bed paddy drying process and performance. **Drying technology**, Taylor & Francis, v. 32, n. 8, p. 919–934, 2014.

FAGHRI, A.; ZHANG, Y.; HOWELL, J. R. **Advanced heat and mass transfer**. [S.l.]: Global Digital Press, 2010.

FAO. **Grain crop drying, handling and storage**. 2010. Accessed = 2019-11-30. Disponível em: <http://www.fao.org/3/i2433e/i2433e10.pdf>.

GOLDSMITH, P. D.; MARTINS, A. G.; MOURA, A. D. de. The economics of post-harvest loss: a case study of the new large soybean-maize producers in tropical brazil. **Food Security**, Springer, v. 7, n. 4, p. 875–888, 2015.

GOYEAU, B. et al. Momentum transport at a fluid–porous interface. **International Journal of Heat and Mass Transfer**, Elsevier, v. 46, n. 21, p. 4071–4081, 2003.

HAMMAMI, F.; MABROUK, S. B.; MAMI, A. Modelling and simulation of heat exchange and moisture content in a cereal storage silo. **Mathematical and Computer Modelling of Dynamical Systems**, Taylor & Francis, v. 22, n. 3, p. 207–220, 2016.

HOLLAR, D. W. Jump conditions. In: ____. **Trajectory Analysis in Health Care**. Cham: Springer International Publishing, 2018. ISBN 978-3-319-59626-6. Disponível em: <https://doi.org/10.1007/978-3-319-59626-6_13>.

HUI, Y. H. **Food drying science and technology: microbiology, chemistry, applications**. [S.l.]: DEStech Publications, Inc, 2008.

IGUAZ, A. et al. Thermophysical properties of medium grain rough rice (lido cultivar) at medium and low temperatures. **European Food Research and Technology - EUR FOOD RES TECHNOL**, v. 217, p. 224–229, 09 2003.

JAMET, D.; CHANDESRIS, M.; GOYEAU, B. On the equivalence of the discontinuous one-and two-domain approaches for the modeling of transport phenomena at a fluid/porous interface. **Transport in porous media**, Springer, v. 78, n. 3, p. 403–418, 2009.

JOSEPH, D.; NIELD, D.; PAPANICOLAOU, G. Nonlinear equation governing flow in a saturated porous medium. **Water Resources Research**, Wiley Online Library, v. 18, n. 4, p. 1049–1052, 1982.

JUE, T.-C. Numerical analysis of vortex shedding behind a porous square cylinder. **International Journal of Numerical Methods for Heat & Fluid Flow**, Emerald Group Publishing Limited, 2004.

KAVIANY, M. **Principles of Heat transfer in Porous Media. 2 ed.** [S.l.]: Springer. New York, 1995.

KAWUYO, U.; AVIARA, N.; OKOLO, D. Effects of moisture content and grain variety on frictional properties and specific heat capacity of acha (fonio) grains. **Nigerian Journal of Technological Research**, Federal University of Technology, Minna, Niger State, Nigeria, v. 14, n. 1, p. 1–7, 2019.

KROKIDA, M.; MARINOS-KOURIS, D.; MUJUMDAR, A. S. Handbook of industrial drying. **Rotary Drying**, p. 151–172, 2006.

KWAK, D.; KIRIS, C. C. Artificial compressibility method. In: **Computation of Viscous Incompressible Flows**. [S.l.]: Springer, 2011. p. 41–77.

KWON, K.; CHOI, H. Control of laminar vortex shedding behind a circular cylinder using splitter plates. **Physics of Fluids**, American Institute of Physics, v. 8, n. 2, p. 479–486, 1996.

LAYTON, W. J.; SCHIEWECK, F.; YOTOV, I. Coupling fluid flow with porous media flow. **SIAM Journal on Numerical Analysis**, SIAM, v. 40, n. 6, p. 2195–2218, 2002.

LEONARD, B. A stable and accurate convective modelling procedure based on quadratic upstream interpolation. **Int. J. Mech. Sci**, v. 16, p. 183–308, 1979.

LIU, S.; MASLIYAH, J. H. Non-linear flows in porous media. **Journal of Non-Newtonian Fluid Mechanics**, Elsevier, v. 86, n. 1-2, p. 229–252, 1999.

MAHDHAOUI, H.; CHESNEAU, X.; LAATAR, A. H. Numerical simulation of flow through a porous square cylinder. **Energy Procedia**, Elsevier, v. 139, p. 785–790, 2017.

MARTINEZ, R. C. Simulation model for drying and cooling of rough rice in fixed-bed. **ASIAN JOURNAL OF POSTHARVEST AND MECHANIZATION**, v. 2, n. 1, p. 11, 2019.

MUJUMDAR, A. S. **Handbook of Industrial Drying**. 3. ed. [S.l.]: CRC Press, 2006. ISBN 9781574446685,1574446681.

____. **Handbook of Industrial Drying**. 4. ed. [S.l.]: CRC Press, 2014. ISBN 1466596651,9781466596658.

NAGHAVI, Z.; MOHEB, A.; ZIAEI-RAD, S. Numerical simulation of rough rice drying in a deep-bed dryer using non-equilibrium model. **Energy Conversion and Management**, Elsevier, v. 51, n. 2, p. 258–264, 2010.

NAZAR, R. et al. The brinkman model for the mixed convection boundary layer flow past a horizontal circular cylinder in a porous medium. **International Journal of Heat and Mass Transfer**, Elsevier, v. 46, n. 17, p. 3167–3178, 2003.

NIELD, D. A.; BEJAN, A. Heat transfer through a porous medium. In: **Convection in porous media**. [S.l.]: Springer, 2017. p. 37–55.

NIELD, D. A.; BEJAN, A. et al. **Convection in porous media**. [S.l.]: Springer, 2006. v. 3.

OCHOA-TAPIA, J. A.; WHITAKER, S. Momentum transfer at the boundary between a porous medium and a homogeneous fluid—i. theoretical development. **International Journal of Heat and Mass Transfer**, Elsevier, v. 38, n. 14, p. 2635–2646, 1995.

PANIGRAHI, S. S. et al. Modeling of heat and mass transfer within the grain storage ecosystem using numerical methods: A review. **Drying Technology**, Taylor & Francis, v. 38, n. 13, p. 1677–1697, 2020.

PARK, D.; LADD, D.; HENDRICKS, E. Feedback control of von kármán vortex shedding behind a circular cylinder at low reynolds numbers. **Physics of fluids**, American Institute of Physics, v. 6, n. 7, p. 2390–2405, 1994.

PARRY, J. Mathematical modelling and computer simulation of heat and mass transfer in agricultural grain drying: A review. **Journal of Agricultural Engineering Research**, Elsevier, v. 32, n. 1, p. 1–29, 1985.

PRADO, M.; ALONSO, L.; PARK, K. Shrinkage of dates (phoenix dactilyfera l.) during drying. **Drying Technology**, Taylor & Francis, v. 18, n. 1-2, p. 295–310, 2000.

RAGHAVAN, V. G. Drying of agriculturai products. In: **Handbook of industrial drying**. [S.l.]: CRC Press, 2020. p. 627–642.

RASHIDI, S. et al. Numerical simulation of forced convective heat transfer past a square diamond-shaped porous cylinder. **Transport in porous media**, Springer, v. 102, n. 2, p. 207–225, 2014.

____. Fluid flow and forced convection heat transfer around a solid cylinder wrapped with a porous ring. **International Journal of Heat and Mass Transfer**, Elsevier, v. 63, p. 91–100, 2013.

RESENDE, O. et al. Bean moisture diffusivity and drying kinetics: a comparison of the liquid diffusion model when taking into account and neglecting grain shrinkage. **Spanish Journal of Agricultural Research**, v. 5, n. 1, p. 51–58, 2007.

RODI, W.; MAJUMDAR, S.; SCHöNUNG, B. Finite volume methods for two-dimensional incompressible flows with complex boundaries. **Computer Methods in Applied Mechanics and Engineering**, v. 75, p. 369 – 392, 1989.

SABLANI, S. S.; RAMASWAMY, H. S. Physical and thermal properties of cereal grains. **Hanbook of Postharvest Technology, eds GSV Raghavan, A. Chakraverty, AS Mujumdar and HS Ramaswamy**, p. 17–40, 2003.

SADAKA, S.; ATUNGULU, G. G.; OLATUNDE, G. **Understanding Grain Shrinkage and Expansion**. [S.l.]: Cooperative Extension Service, University of Arkansas, 2016.

SEIFI, M. R.; ALIMARDANI, R. The moisture content effect on some physical and mechanical properties of corn (sc 704). **Journal of Agricultural Science**, Canadian Center of Science and Education, v. 2, n. 4, p. 125, 2010.

SIIKONEN MM RAHMAN, T. An artificial compressibility method for incompressible flows. **Numerical Heat Transfer, Part B: Fundamentals**, Taylor & Francis, v. 40, n. 5, p. 391–409, 2001.

SILVA, R. A.; LEMOS, M. J. de. Numerical analysis of the stress jump interface condition for laminar flow over a porous layer. **Numerical Heat Transfer: Part A: Applications**, Taylor & Francis, v. 43, n. 6, p. 603–617, 2003.

SITOMPUL, J. P.; ISTADI; SUMARDIONO, S. Modelling and simulation of momentum, heat, and mass transfer in a deep-bed grain dryer. **Drying Technology**, Taylor & Francis, v. 21, n. 2, p. 217–229, 2003.

SRIVASTAVA, V.; JOHN, J. Deep bed grain drying modeling. **Energy conversion and management**, Elsevier, v. 43, n. 13, p. 1689–1708, 2002.

SUN, D.-W.; WOODS, J. Simulation of the heat and moisture transfer process during drying in deep grain beds. **Drying Technology**, Taylor & Francis, v. 15, n. 10, p. 2479–2492, 1997.

TAVMAN, S.; TAVMAN, I. Measurement of effective thermal conductivity of wheat as a function of moisture content. **International communications in heat and mass transfer**, Pergamon, v. 25, n. 5, p. 733–741, 1998.

THORPE, G. R. The application of computational fluid dynamics codes to simulate heat and moisture transfer in stored grains. Elsevier, v. 44, n. 1, p. 21–31, 2008.

VERSTEEG, H. K.; MALALASEKERA, W. **An introduction to computational fluid dynamics: the finite volume method**. [S.l.]: Pearson education, 2007.

VERSTEEG H. K.; MALALASEKERA, W. **An Introduction to Computational Fluid Dynamics: The Finite Volume Method. 2 ed.** [S.l.]: Pearson Prentice Hall, 2007.

ZARE D; MINAEI, S. Z. M.; KAOSHTAGHAZA, M. Computer simulation of rough rice drying in a batch dryer. **Energy Conversion and Management**, Elsevier, v. 47, n. 18-19, p. 3241–3254, 2006.

ZDRAVKOVICH, M. M. **Flow around circular cylinders: Volume 2: Applications**. [S.l.]: Oxford university press, 1997. v. 2.

ZHANG, K. et al. Numerical study on the effect of shape modification to the flow around circular cylinders. **Journal of Wind Engineering and Industrial Aerodynamics**, Elsevier, v. 152, p. 23–40, 2016.